Molecular mechanism of microtubule nucleation from gamma-tubulin ring complex

Akanksha Thawani[1], Howard A Stone[2], Joshua W Shaevitz[3,4], Sabine Petry[5,*]

[1]Department of Chemical and Biological Engineering, Princeton University

[2]Department of Mechanical and Aerospace Engineering, Princeton University

[3]Lewis-Sigler Institute for Integrative Genomics, Princeton University

[4]Department of Physics, Princeton University

[5]Department of Molecular Biology, Princeton University, United States

* Correspondence to: Sabine Petry (spetry@princeton.edu)

Abstract

Determining how microtubules (MTs) are nucleated is essential for understanding how the cytoskeleton assembles. Yet, half a century after the discovery of MTs and αβ-tubulin subunits and decades after the identification of the γ-tubulin ring complex (γ-TuRC) as the universal MT nucleator, the underlying mechanism largely remains a mystery. Using single molecule studies, we uncover that γ-TuRC nucleates a MT more efficiently than spontaneous assembly. The laterally interacting array of γ-tubulins on γ-TuRC facilitates the lateral association of αβ-tubulins, while longitudinal affinity between γ/αβ-tubulin is surprisingly weak. During nucleation, 3-4 αβ-tubulin dimers bind stochastically to γ-TuRC on average until two of them create a lateral contact and overcome the nucleation barrier. Although γ-TuRC defines the nucleus, XMAP215 significantly increases reaction efficiency by facilitating αβ-tubulin incorporation. In sum, we elucidate how MT initiation occurs from γ-TuRC and determine how it is regulated.

Introduction

Microtubules (MTs) enable cell division, motility, intracellular organization and transport. MTs were found to consist of αβ-tubulin dimers fifty years ago, yet, how MTs are nucleated in the cell to build the cytoskeleton remains poorly understood[1–3].

MTs assemble spontaneously from αβ-tubulin subunits *in vitro* via the cooperative assembly of many tubulin dimers and hence this process displays a kinetic barrier[4–8]. Consequently, spontaneous MT nucleation is rarely observed in cells[9,10]. Instead, the major MT nucleator γ-tubulin is required *in vivo*[9–11]. γ-tubulin forms a 2.2 megadalton, ring-shaped complex with γ-tubulin complex proteins (GCPs), known as the γ-Tubulin Ring Complex (γ-TuRC) [12–16]. γ-TuRC has been proposed to template the assembly of αβ-tubulin dimers into a ring, resulting in nucleation of a MT[15–21]. However, kinetic measurements that provide direct evidence for this hypothesis have been lacking and several important questions about how γ-TuRC nucleates MTs have remained unanswered.

In the absence of purified γ-TuRC and an assay to visualize MT nucleation events from single γ-TuRC molecules in real time, recent studies used alternative MT assembly sources, such as spontaneous MT assembly or stabilized MTs with blunt ends hypothesized to resemble the γ-TuRC interface. Based on these alternatives, competition between growth and catastrophe of the nascent plus-end was proposed to yield the nucleation barrier in the cell[22,23], but this has not been examined with the nucleator γ-TuRC. Recently, the MT polymerase XMAP215 was identified as an essential MT nucleation factor *in vivo*, which synergistically nucleates MTs with γ-TuRC[24–26]. Yet, the specific roles of XMAP215 and γ-TuRC in MT nucleation have yet to be discovered.

To explore the mechanism of MT nucleation, we reconstituted and visualized MT nucleation by γ-TuRC live with single molecule resolution. We uncover the molecular composition of the

47 MT nucleus, and determine the roles XMAP215 and γ-TuRC in MT nucleation.

48

Results

Reconstituting and visualizing microtubule nucleation from γ-TuRC

To study how γ-TuRC nucleates MTs (Fig. 1A), we purified endogenous γ-TuRC from *Xenopus* egg extracts and biotinylated the complexes to immobilize them on functionalized glass (Fig. S1A-C). Upon perfusing fluorescent αβ-tubulin, we visualized MT nucleation live with total internal reflection fluorescence microscopy (TIRFM). Strikingly, MT nucleation events occurred specifically from single γ-TuRC molecules (Fig. 1B; Fig. S1D and Movie S1-2). Kymographs revealed that attached γ-TuRC assembled αβ-tubulin into a MT *de novo* starting from zero length within the diffraction limit of light microscopy (Fig. 1C), ruling out an alternative model where MTs first spontaneously nucleate and then become stabilized via γ-TuRC. By observing the fiduciary marks on the MT lattice (Fig. 1C) and generating polarity-marked MTs from attached γ-TuRC (Fig. S1E), we showed that γ-TuRC caps the MT minus-end, while only the plus-end polymerizes. Altogether, our results show that γ-TuRC directly nucleates MTs.

Defining the microtubule nucleus on γ-TuRC

To determine how γ-TuRC nucleates MTs, we measured the kinetics of MT nucleation for a constant density of γ-TuRC and increasing αβ-tubulin concentration (Fig. 1D and Movie S3). Surprisingly, γ-TuRC nucleated MTs starting from 7 μM tubulin (Fig. 1D), which is higher than the minimum tubulin concentration (C^*) needed for growth at pre-formed MT plus-ends ($C^* = 1.4$ μM, Fig. 1E). Furthermore, the number of MTs nucleated from γ-TuRC increased non-linearly with tubulin concentration as opposed to the linear increase in MT's growth-speed with tubulin concentration (Fig. 1E). By measuring the number of MTs nucleated over time with varying αβ-

72 tubulin concentration (Fig. 1F), we calculated the rate of MT nucleation. The power-law
73 dependence on tubulin concentration (Fig. 1G) yields the number of αβ-tubulin dimers, 3.7 ± 0.5,
74 that initiate MT assembly from γ-TuRC (Fig. 1G). Thus, the cooperative assembly of 3-4 tubulin
75 subunits on γ-TuRC represents the most critical, rate-limiting step in MT nucleation.
76
77 **Efficiency of γ-TuRC-mediated nucleation**
78 Based on the traditional, fixed, end-point assays for MT nucleation with large error margins, γ-
79 TuRC was believed to be a poor nucleator[14]. To measure the efficiency of γ-TuRC-mediated MT
80 nucleation, we compared it with spontaneous MT nucleation in our live TIRFM assay (Fig. 1H).
81 In contrast to γ-TuRC-mediated nucleation, a high concentration of 14 μM tubulin was required
82 for spontaneous assembly of MTs, after which both the plus- and minus-ends polymerize (Fig. 1H,
83 Fig. S1F and Movie S4). The number of MTs assembled as a function of the αβ-tubulin
84 concentration displayed a power-law dependence with the exponent of 8 ± 1 (Fig. 1I), indicating
85 a highly cooperative process that requires 8 αβ-tubulin dimers in a rate-limiting intermediate, in
86 agreement with previous reports (Fig. 1H schematic, refs 4,8). In conclusion, γ-TuRC nucleates
87 MTs significantly more efficiently (Fig. S1G), because its critical nucleus requires less than half
88 the number of αβ-tubulin dimers compared to spontaneous assembly.
89
90 **Does γ-TuRC nucleate a microtubule via the blunt plus-end model?**
91 It has been widely proposed that the γ-tubulin ring on γ-TuRC resembles the blunt plus-end of a
92 MT formed by a ring of αβ-tubulins[20,22,27]. To test this proposition, we generated stabilized MT
93 seeds with blunt ends as described recently[22] and observed MT assembly from αβ-tubulin dimers
94 (Fig. 2A). At a minimum concentration of 2.45 μM, approaching the critical concentration needed

95 for polymerization, a large proportion of pre-formed MT seeds assembled MTs immediately (Fig.
96 S2A-B, Fig. 2A and Movie S5). The measured reaction kinetics (Fig. 2B) as a function of the αβ-
97 tubulin concentration was used to obtain a power-law of the nucleation rate, 1.2 ± 0.4 (Fig. 2C).
98 This demonstrates that blunt MT seeds assemble tubulin dimers into a lattice in a non-cooperative
99 manner, where a single αβ-tubulin dimer suffices to overcome the rate-limiting step resembling
100 the polymerization of a MT. Thus, the kinetics of γ-TuRC-mediated MT nucleation does not
101 resemble a blunt MT plus-end.
102
103 **Molecular insight into microtubule nucleation by γ-TuRC**
104 We hypothesized that γ-tubulin's binding properties with αβ-tubulin at the nucleation interface γ-
105 TuRC could provide insight into the mechanism of nucleation. We purified γ-tubulin, which
106 assembles into higher order oligomers in physiological buffer [24] and strikingly, into filaments at
107 high γ-tubulin concentrations (Fig. S2C). Because γ-tubulins have been shown to arrange laterally,
108 as observed previously in its crystallized form[28], a plus-ends outward orientation of γ-tubulin
109 molecules could form a nucleation interface.
110 Surprisingly, the γ-tubulin oligomers efficiently nucleated MTs from αβ-tubulin subunits
111 (Fig. 2D and Movie S6) and even more strikingly, capped MT minus-ends while allowing newly
112 generated MT plus-ends to polymerize (Fig. 2E). This activity is similar to that of γ-TuRC,
113 suggesting that lateral γ-tubulin arrays on the nucleation interface of γ-TuRC are sufficient to
114 nucleate MTs.
115 Knowing that lateral γ-tubulin arrays in purified γ-tubulin oligomers and within γ-TuRC
116 nucleate MTs, we hypothesized that the longitudinal affinity between γ-tubulin and αβ-tubulin at
117 the interface of γ-TuRC could be critical in regulating its nucleation efficiency. Using biolayer

118 interferometry, we compared the interaction of αβ-tubulin dimers with themselves versus with γ-
119 tubulin. Specific interactions between probe-bound αβ-tubulin and increasing concentrations of
120 unlabeled αβ-tubulin were measured (Fig. 2F), which must be longitudinal based on the observed
121 protofilaments in the αβ-tubulin sample by EM (Fig. S2D). In contrast, no significant binding
122 between monomeric γ-tubulin and αβ-tubulin was detected (Fig. 2F), suggesting that the
123 heterogenous longitudinal affinity between γ-tubulin and αβ-tubulin on the nucleation interface
124 may be weaker compared to αβ-tubulin with another αβ-tubulin molecule that occurs when the
125 MT lattice polymerizes. In sum, the difference in interaction strength is the basis for the kinetic
126 barrier we observed with γ-TuRC but not with a blunt MT plus-end, which we summarize with an
127 interface interaction model (Fig. 2G).

128 We next asked how 3-4 tubulin dimers formed the rate-limiting species during γ-TuRC
129 nucleation. In stochastic simulations, the 13 available binding sites on γ-tubulin molecules within
130 γ-TuRC were allowed to be occupied at random with αβ-tubulin subunits. We then assessed how
131 many αβ-tubulin dimers need to assemble on γ-TuRC to obtain two αβ-tubulin molecules on
132 neighboring sites and form a favorable configuration with a lateral contact between the two αβ-
133 tubulins (Fig. 2H). The simulations show that 3.7 ± 1 tubulin dimers assemble on γ-TuRC to form
134 the first lateral contact between two αβ-tubulins (Fig. 2H), in striking agreement with the critical
135 nucleus size we measured. In sum, our data shows that a lateral γ-tubulin array positioned by γ-
136 TuRC promotes MT nucleation. The low γ-tubulin:αβ-tubulin affinity requires binding of 3-4 αβ-
137 tubulin dimers to γ-TuRC to form the first lateral contact between two αβ-tubulin dimers and
138 overcome the kinetic barrier before entering the MT polymerization phase. This nucleation barrier,
139 in turn, provides the ability to further modulate MT nucleation via other factors.
140

141 **Regulation of γ-TuRC mediated nucleation by microtubule associated proteins**

142 Recent work suggested that MT-associated proteins (MAPs), which stabilize or destabilize MT
143 plus-ends, influence MT nucleation in an analogous fashion[7,22,23,27]. We assessed this hypothesis
144 for MT nucleation by γ-TuRC. The protein TPX2 functions as an anti-catastrophe factor *in vitro*
145 [22,23] and has been suggested to directly stimulate γ-TuRC-mediated nucleation[21,29–31]. Strikingly,
146 although TPX2 binds along the MT lattice, it does not increase nucleation activity of γ-TuRC (Fig.
147 3A and Movie S7). Similarly, the catastrophe factor EB1 does not decrease the nucleation activity
148 of γ-TuRC (Fig. S3A and Movie S8). Thus, in agreement with our previous results (Figs. 1 and
149 2A-B), destabilization of MT plus-ends and a competition between
150 polymerization/depolymerization is not sufficient to explain the properties of MT nucleation from
151 γ-TuRC. Not surprisingly, decreasing the net rate of incorporation of tubulin into a MT using
152 Stathmin, which sequesters tubulin dimers[32,33], or MCAK, which removes tubulin dimers from the
153 MT lattice and prevents polymerization[34,35], decreased the number of MTs generated from γ-TuRC
154 (Fig. S3B).

155

156 **How do γ-TuRC and XMAP215 synergistically nucleate microtubules?**

157 At low tubulin concentration of 3.5 μM and 7 μM, where either none or very little MT nucleation
158 occurs from γ-TuRCs alone respectively, the addition of XMAP215 induced many surface-
159 attached γ-TuRCs to nucleate MTs resulting in significant increase in MT nucleation rate (Fig. 3B-
160 C and Movie S9). XMAP215 effectively decreases the minimal tubulin concentration necessary
161 for MT nucleation from γ-TuRC to 1.6 μM, which is very close to that needed for plus-end
162 polymerization. What is the sequence of events that leads to synergistic MT nucleation? By
163 directly visualizing γ-TuRC and XMAP215 molecules during the nucleation reaction, we found

164 that XMAP215 and γ-TuRC molecules first formed a complex from which a MT was nucleated
165 (Fig. 3D and Movie S11). For 76% of the events (n=56), XMAP215 visibly persisted between 3
166 to over 300 seconds on γ-TuRC before MT nucleation, and with a 50% probability XMAP215
167 remained on the minus-end together with γ-TuRC (n=58).

168 Could XMAP215 accelerate nucleation by altering the critical tubulin nucleus that
169 assembles during γ-TuRC-mediated nucleation? Titrating tubulin at constant γ-TuRC and
170 XMAP215 concentrations (Fig. S4A and Movies S10) yielded a similar power-law dependence
171 between the MT nucleation rate and tubulin concentration (Fig. 3E). The resulting critical nucleus
172 size of 3.2 ± 1.2 is very similar to that for γ-TuRC alone (Fig. 3E). Moreover, the C-terminus of
173 XMAP215 (TOG5 and C-terminal domain), which directly interacts with γ-tubulin but not with
174 αβ-tubulin[24], does not enhance MT nucleation from γ-TuRC (Fig. S4B). Altogether, γ-TuRC
175 determines the critical nucleus of αβ-tubulin dimers for MT nucleation (Fig. 2H). XMAP215,
176 which directly binds to γ-tubulin via its C-terminal domain, does not appear to activate γ-TuRC
177 via a conformational change, but likely relies on N-terminal TOG domains to increase αβ-tubulin
178 incorporation by effectively increasing the local αβ-tubulin concentration, and thereby promoting
179 MT nucleation.
180

181 **Discussion**

182 Decades after the discovery of αβ-tubulin and MTs and the identification of γ-TuRC as the
183 universal MT nucleator[17–19], it has remained poorly understood how MTs are being nucleated[7,20,21].
184 Here, we show that γ-TuRC-mediated MT nucleation is more efficient than spontaneous MT
185 assembly, requiring fewer tubulin dimers to form the rate-limiting reaction intermediate. This
186 explains why MTs do not form spontaneously in the cell and why γ-TuRC is essential, addressing
187 a long debate on γ-TuRC's MT nucleation activity and requirement[36–38]. Spontaneous MT
188 assembly requires higher tubulin concentrations and occurs due to stronger longitudinally-
189 interacting αβ/αβ-tubulin and weaker lateral interactions. In contrast, γ-TuRC-mediated
190 nucleation, driven by the lateral adjacency of the γ-tubulins on the nucleation interface, is sufficient
191 to overcome the intrinsically very weak αβ-tubulin lateral interaction, thereby potentiating MT
192 nucleation. Thus, we propose that, in metazoans analogous to the *S. cerevisiae* γ-TuSC rings[15,16],
193 GCPs within γ-TuRC restrict the number of laterally-arranged γ-tubulin subunits, and position
194 them in the right geometry to template 13-pf MTs. Finally, our results show that 3-4 αβ-tubulin
195 form the critical nucleus on γ-TuRC, not 1 or 13 which would have been expected from previous
196 mechanistic hypotheses[20]. We find that on average 3-4 αβ-tubulin dimers assemble on γ-TuRC to
197 form the first lateral αβ-/αβ-tubulin contact and overcome the kinetic barrier that results from low
198 longitudinal affinity between γ-:αβ-tubulin on γ-TuRC. However, alternative reaction
199 intermediates during nucleation from γ-TuRC may exist. In the future, it will be important to
200 visualize the nucleation intermediates on γ-TuRC, develop molecular simulations with
201 experimentally derived affinities at various interaction interfaces and evaluate whether additional
202 effects from tubulin straightening play a significant role in MT nucleation in the cell.

203 The intermediate level of MT nucleation efficiency afforded by γ-TuRC allows other
204 factors to further modulate its efficiency. As such, XMAP215 accelerates MT nucleation from γ-
205 TuRC, while not altering the geometry of the αβ-tubulin nucleus on γ-TuRC or directly activating
206 γ-TuRC. Future studies will be necessary to define the modes by which XMAP215 contributes to
207 γ-TuRC-mediated MT nucleation, such as increasing the probability of the γ/αβ-tubulin interaction
208 or promoting straightening of incoming tubulin dimers. Our findings suggest that influencing γ/αβ-
209 tubulin interaction favorably or unfavorably may underlie a dominant mechanism for regulating
210 nucleation in the cell by other, yet unidentified nucleation factors. Additionally, γ-TuRC's activity
211 is further regulated via accessory proteins such as CDK5RAP2, and NME7[2,20,39,40]. While the
212 mechanisms of these additional regulation layers are yet to be defined, the insights on MT
213 nucleation by γ-TuRC and XMAP215 provide an essential basis to build upon. Finally, this work
214 opens the door to reconstitute cellular structures *in vitro* using MT nucleation from γ-
215 TuRC/XMAP215 to further our understanding of how the cytoskeleton is generated to support cell
216 function.

Supplementary Information

Supplementary Information includes four figures and ten videos.

Acknowledgements

We thank David Agard, Tim Mitchison, Michelle Moritz and Petry lab members for discussions. This work was supported by an American Heart Association predoctoral fellowship 17PRE33660328 and a Princeton University Honorific Fellowship (both to AT), the NIH New Innovator Award 1DP2GM123493, Pew Scholars Program in the Biomedical Sciences 00027340, David and Lucile Packard Foundation 2014-40376 (all to SP), and the Center for the Physics of Biological Function sponsored by the National Science Foundation grant PHY-1734030.

Author contributions

A.T. designed and performed research, analyzed the data and wrote the manuscript. S.P., J.W.S. and H.A.S. supervised research and wrote the manuscript.

Competing financial interests

The authors declare no competing financial interests.

Abbreviations List

Microtubule (MT)

Microtubule associated protein (MAP)

Gamma-tubulin (γ-tubulin) and Gamma-tubulin ring complex (γ-TuRC)

Gamma-tubulin complex protein (GCP)

240 Protofilament (pf)

241 Electron microscopy (EM)

242 **References**

243 1. Brugués, J., Nuzzo, V., Mazur, E. & Needleman, D. J. Nucleation and transport organize
244 microtubules in metaphase spindles. *Cell* **149**, 554–564 (2012).
245 2. Petry, S. & Vale, R. D. Microtubule nucleation at the centrosome and beyond. *Nat. Cell Biol.*
246 **17**, 1089–1093 (2015).
247 3. Wu, J. & Akhmanova, A. Microtubule-Organizing Centers. *Annu. Rev. Cell Dev. Biol.* **33**, 51–
248 75 (2017).
249 4. Voter, W. A. & Erickson, H. P. The kinetics of microtubule assembly. Evidence for a two-
250 stage nucleation mechanism. *J. Biol. Chem.* **259**, 10430–10438 (1984).
251 5. Portran, D., Schaedel, L., Xu, Z., Théry, M. & Nachury, M. V. Tubulin acetylation protects
252 long-lived microtubules against mechanical ageing. *Nat. Cell Biol.* **19**, 391–398 (2017).
253 6. Rice, L., Moritz, M. & Agard, D. A. *Microtubules form by progressively faster tubulin*
254 *accretion, not by nucleation-elongation*. http://biorxiv.org/lookup/doi/10.1101/545236
255 (2019) doi:10.1101/545236.
256 7. Roostalu, J. & Surrey, T. Microtubule nucleation: beyond the template. *Nat. Rev. Mol. Cell*
257 *Biol.* **18**, 702–710 (2017).
258 8. Flyvbjerg, H., Jobs, E. & Leibler, S. Kinetics of self-assembling microtubules: an 'inverse
259 problem' in biochemistry. *Proc. Natl. Acad. Sci. U.S.A.* **93**, 5975–5979 (1996).
260 9. Hannak, E. *et al.* The kinetically dominant assembly pathway for centrosomal asters in
261 Caenorhabditis elegans is gamma-tubulin dependent. *J. Cell Biol.* **157**, 591–602 (2002).
262 10. Groen, A. C., Maresca, T. J., Gatlin, J. C., Salmon, E. D. & Mitchison, T. J. Functional
263 overlap of microtubule assembly factors in chromatin-promoted spindle assembly. *Mol. Biol.*
264 *Cell* **20**, 2766–2773 (2009).

265 11. Oakley, C. E. & Oakley, B. R. Identification of gamma-tubulin, a new member of the tubulin
266 superfamily encoded by mipA gene of Aspergillus nidulans. *Nature* **338**, 662–664 (1989).
267 12. Moritz, M., Braunfeld, M. B., Sedat, J. W., Alberts, B. & Agard, D. A. Microtubule
268 nucleation by gamma-tubulin-containing rings in the centrosome. *Nature* **378**, 638–640
269 (1995).
270 13. Moritz, M., Zheng, Y., Alberts, B. M. & Oegema, K. Recruitment of the gamma-tubulin ring
271 complex to Drosophila salt-stripped centrosome scaffolds. *J. Cell Biol.* **142**, 775–786 (1998).
272 14. Zheng, Y., Wong, M. L., Alberts, B. & Mitchison, T. Nucleation of microtubule assembly by
273 a gamma-tubulin-containing ring complex. *Nature* **378**, 578–583 (1995).
274 15. Kollman, J. M., Polka, J. K., Zelter, A., Davis, T. N. & Agard, D. A. Microtubule nucleating
275 gamma-TuSC assembles structures with 13-fold microtubule-like symmetry. *Nature* **466**,
276 879–882 (2010).
277 16. Kollman, J. M. *et al.* Ring closure activates yeast γTuRC for species-specific microtubule
278 nucleation. *Nat. Struct. Mol. Biol.* **22**, 132–137 (2015).
279 17. Moritz, M., Braunfeld, M. B., Guénebaut, V., Heuser, J. & Agard, D. A. Structure of the
280 gamma-tubulin ring complex: a template for microtubule nucleation. *Nat. Cell Biol.* **2**, 365–
281 370 (2000).
282 18. Keating, T. J. & Borisy, G. G. Immunostructural evidence for the template mechanism of
283 microtubule nucleation. *Nat. Cell Biol.* **2**, 352–357 (2000).
284 19. Wiese, C. & Zheng, Y. A new function for the gamma-tubulin ring complex as a microtubule
285 minus-end cap. *Nat. Cell Biol.* **2**, 358–364 (2000).
286 20. Kollman, J. M., Merdes, A., Mourey, L. & Agard, D. A. Microtubule nucleation by γ-tubulin
287 complexes. *Nat. Rev. Mol. Cell Biol.* **12**, 709–721 (2011).

288 21. Tovey, C. A. & Conduit, P. T. Microtubule nucleation by γ-tubulin complexes and beyond.
289 *Essays Biochem.* **62**, 765–780 (2018).
290 22. Wieczorek, M., Bechstedt, S., Chaaban, S. & Brouhard, G. J. Microtubule-associated
291 proteins control the kinetics of microtubule nucleation. *Nat. Cell Biol.* **17**, 907–916 (2015).
292 23. Roostalu, J., Cade, N. I. & Surrey, T. Complementary activities of TPX2 and chTOG
293 constitute an efficient importin-regulated microtubule nucleation module. *Nat. Cell Biol.* **17**,
294 1422–1434 (2015).
295 24. Thawani, A., Kadzik, R. S. & Petry, S. XMAP215 is a microtubule nucleation factor that
296 functions synergistically with the γ-tubulin ring complex. *Nat. Cell Biol.* **20**, 575–585
297 (2018).
298 25. Flor-Parra, I., Iglesias-Romero, A. B. & Chang, F. The XMAP215 Ortholog Alp14 Promotes
299 Microtubule Nucleation in Fission Yeast. *Curr. Biol.* **28**, 1681-1691.e4 (2018).
300 26. Gunzelmann, J. *et al.* The microtubule polymerase Stu2 promotes oligomerization of the γ-
301 TuSC for cytoplasmic microtubule nucleation. *Elife* **7**, (2018).
302 27. Brouhard, G. J. & Rice, L. M. Microtubule dynamics: an interplay of biochemistry and
303 mechanics. *Nat. Rev. Mol. Cell Biol.* **19**, 451–463 (2018).
304 28. Aldaz, H., Rice, L. M., Stearns, T. & Agard, D. A. Insights into microtubule nucleation from
305 the crystal structure of human gamma-tubulin. *Nature* **435**, 523–527 (2005).
306 29. Alfaro-Aco, R., Thawani, A. & Petry, S. Structural analysis of the role of TPX2 in branching
307 microtubule nucleation. *J. Cell Biol.* **216**, 983–997 (2017).
308 30. Zhang, R., Roostalu, J., Surrey, T. & Nogales, E. Structural insight into TPX2-stimulated
309 microtubule assembly. *Elife* **6**, (2017).

310 31. Wiese, C. & Zheng, Y. Microtubule nucleation: gamma-tubulin and beyond. *J. Cell. Sci.*
311 **119**, 4143–4153 (2006).
312 32. Jourdain, L., Curmi, P., Sobel, A., Pantaloni, D. & Carlier, M. F. Stathmin: a tubulin-
313 sequestering protein which forms a ternary T2S complex with two tubulin molecules.
314 *Biochemistry* **36**, 10817–10821 (1997).
315 33. Belmont, L. D. & Mitchison, T. J. Identification of a protein that interacts with tubulin
316 dimers and increases the catastrophe rate of microtubules. *Cell* **84**, 623–631 (1996).
317 34. Howard, J. & Hyman, A. A. Microtubule polymerases and depolymerases. *Curr. Opin. Cell*
318 *Biol.* **19**, 31–35 (2007).
319 35. Hunter, A. W. *et al.* The kinesin-related protein MCAK is a microtubule depolymerase that
320 forms an ATP-hydrolyzing complex at microtubule ends. *Mol. Cell* **11**, 445–457 (2003).
321 36. Rogers, G. C., Rusan, N. M., Peifer, M. & Rogers, S. L. A multicomponent assembly
322 pathway contributes to the formation of acentrosomal microtubule arrays in interphase
323 Drosophila cells. *Mol. Biol. Cell* **19**, 3163–3178 (2008).
324 37. Raff, J. W. Phase Separation and the Centrosome: A Fait Accompli? *Trends Cell Biol.* **29**,
325 612–622 (2019).
326 38. Woodruff, J. B. *et al.* The Centrosome Is a Selective Condensate that Nucleates Microtubules
327 by Concentrating Tubulin. *Cell* **169**, 1066-1077.e10 (2017).
328 39. Choi, Y.-K., Liu, P., Sze, S. K., Dai, C. & Qi, R. Z. CDK5RAP2 stimulates microtubule
329 nucleation by the gamma-tubulin ring complex. *J. Cell Biol.* **191**, 1089–1095 (2010).
330 40. Liu, P., Choi, Y.-K. & Qi, R. Z. NME7 is a functional component of the γ-tubulin ring
331 complex. *Mol. Biol. Cell* **25**, 2017–2025 (2014).

332 41. Petry, S., Pugieux, C., Nédélec, F. J. & Vale, R. D. Augmin promotes meiotic spindle
333 formation and bipolarity in Xenopus egg extracts. *Proc. Natl. Acad. Sci. U.S.A.* **108**, 14473–
334 14478 (2011).
335 42. Tan, S., Kern, R. C. & Selleck, W. The pST44 polycistronic expression system for producing
336 protein complexes in Escherichia coli. *Protein Expr. Purif.* **40**, 385–395 (2005).
337 43. Ohi, R., Sapra, T., Howard, J. & Mitchison, T. J. Differentiation of cytoplasmic and meiotic
338 spindle assembly MCAK functions by Aurora B-dependent phosphorylation. *Mol. Biol. Cell*
339 **15**, 2895–2906 (2004).
340 44. Reber, S. B. *et al.* XMAP215 activity sets spindle length by controlling the total mass of
341 spindle microtubules. *Nat. Cell Biol.* **15**, 1116–1122 (2013).
342 45. Hannak, E. & Heald, R. Investigating mitotic spindle assembly and function in vitro using
343 Xenopus laevis egg extracts. *Nat Protoc* **1**, 2305–2314 (2006).
344 46. Murray, A. W. & Kirschner, M. W. Cyclin synthesis drives the early embryonic cell cycle.
345 *Nature* **339**, 275–280 (1989).
346 47. Bieling, P., Telley, I. A., Hentrich, C., Piehler, J. & Surrey, T. Fluorescence microscopy
347 assays on chemically functionalized surfaces for quantitative imaging of microtubule, motor,
348 and +TIP dynamics. *Methods Cell Biol.* **95**, 555–580 (2010).
349

350 **Methods**

351

352 **Purification of recombinant proteins**

353 C-terminal GFP was replaced with mCherry tag in the pET21a vector carrying EB1[41]. Full-length
354 TPX2 with N-terminal Strep II-6xHis-GFP-TEV site tags was cloned into pST50Tr-
355 STRHISNDHFR (pST50) vector[42] using Gibson Assembly (New England Biolabs). N-terminal
356 6xHis-tagged, *Xenopus laevis* Stathmin 1A was a gift from Christiane Wiese (University of
357 Madison). N-terminal tagged 6xHis-TEV MCAK plasmid was a gift from Ryoma Ohi[43]. Wild-
358 type XMAP215 with C-terminal GFP-7xHis plasmid was a gift from Simone Reber[44] and was used
359 to clone XMAP215 with C-terminal SNAP-TEV-7xHis-StrepII tags, first into pST50 vector and
360 further into pFastBac1 vector. TOG5-CT truncation of XMAP215 was produced by cloning amino
361 acids 1091-2065 into pST50 vector with C-terminal GFP-7xHis-Strep tags. Human γ-tubulin TEV-
362 Strep II-6xHis tags was codon-optimized for Sf9 expression, synthesized (Genscript), and further
363 cloned into pFastBac1 vector.

364 EB1, TPX2, Stathmin and XMAP215 TOG5-CT used in this study were expressed in *E.*
365 *coli* Rosetta2 cells (EMD Millipore) by inducing with 0.5-1 mM IPTG for 12-18 hours at 16°C or
366 7 hours at 25°C. Wild-type XMAP215, MCAK and γ-tubulin were expressed and purified from
367 Sf9 cells using Bac-to-Bac system (Invitrogen). The cells were lysed (EmulsiFlex, Avestin) and
368 *E. coli* lysate was clarified by centrifugation at 13,000 rpm in Fiberlite F21-8 rotor (ThermoFisher)
369 and Sf9 cell lysate at 50,000 rpm in Ti70 rotor (Beckman Coulter) for 30-45 minutes.

370 EB1 and Stathmin were purified using His-affinity (His-Trap HP, GE Healthcare) by first
371 binding in binding buffer (20mM $NaPO_4$ pH 8.0, 500mM NaCl, 30mM Imidazole, 2.5mM PMSF,
372 6mM BME) and eluting with 300mM Imidazole, followed by gel filtration (HiLoad 16/600

373 Superdex, GE Healthcare) into CSF-XB buffer (100mM KCl, 10mM K-HEPES, 5mM K-EGTA,
374 1mM $MgCl_2$, 0.1mM $CaCl_2$, pH 7.7 with 10% w/v sucrose).

375 TPX2 was first affinity purified using Ni-NTA beads in binding buffer (50mM Tris-HCl
376 pH 8.0, 750mM NaCl, 15mM Imidazole, 2.5mM PMSF, 6mM BME) and eluted with 200mM
377 Imidazole. All protein was pooled and diluted 4-fold to 200mM final NaCl. Nucleotides were
378 removed with a Heparin column (HiTrap Heparin HP, GE Healthcare) by binding protein in
379 250mM NaCl and isocratic elution in 750mM NaCl, all solutions prepared in Heparin buffer
380 (50mM Tris-HCl, pH 8.0, 2.5mM PMSF, 6mM BME). Peak fractions were pooled and loaded on
381 to Superdex 200 pg 16/600, and gel filtration was performed in CSF-XB buffer.

382 MCAK was first affinity purified by binding to His-Trap HP (GE Healthcare) in binding
383 buffer (50mM NaPO4, 500mM NaCl, 6mM BME, 0.1mM MgATP, 10mM Imidazole, 1mM
384 MgCl2, 2.5mM PMSF, 6mM BME, pH to 7.5), eluting with 300mM Imidazole, followed by gel-
385 filtration (Superdex 200 10/300 GL, GE Healthcare) in storage buffer (10 mM K-HEPES pH 7.7,
386 300 mM KCl, 6mM BME, 0.1 mM MgATP, 1mM $MgCl_2$, 10% w/v sucrose).

387 XMAP215-GFP was purified using His-affinity (His-Trap, GE Healthcare) by binding in
388 buffer (50mM $NaPO_4$, 500mM NaCl, 20mM Imidazole, pH 8.0) and eluting in 500mM Imidazole.
389 Peak fractions were pooled and diluted 5-fold with 50mM Na-MES pH 6.6, bound to a cation-
390 exchange column (Mono S 10/100 GL, GE Healthcare) with 50mM MES, 50mM NaCl, pH 6.6
391 and eluted with a salt-gradient up to 1M NaCl. Peak fractions were pooled and dialyzed into CSF-
392 XB buffer. SNAP-tagged XMAP215 was first affinity purified with StrepTrap HP (GE Healthcare)
393 with binding buffer (50mM $NaPO_4$, 270mM NaCl, 2mM $MgCl_2$, 2.5mM PMSF, 6mM BME, pH
394 7.2), eluted with 2.5mM D-desthiobiotin, and cation-exchanged (Mono S 10/100 GL). Peak
395 fractions were pooled, concentrated and reacted with 2-molar excess SNAP-substrate Alexa-488

396 dye (S9129, NEB) overnight at 4°C, followed by purification via gel filtration (Superdex 200
397 10/300 GL) in CSF-XB buffer. Approximately 70% labeling efficiency of the SNAP-tag was
398 achieved.

399 γ-tubulin was purified by binding to HisTrap HP (GE Healthcare) in binding buffer (50
400 mM KPO_4 pH 8.0, 500 mM KCl, 1 mM $MgCl_2$, 10% glycerol, 5mM Imidazole, 0.25 μM GTP, 5
401 mM BME, 2.5mM PMSF), washing first with 50 mM KPO_4 pH 8.0, 300 mM KCl, 1 mM $MgCl_2$,
402 10% glycerol, 25 mM imidazole, 0.25 μM GTP, 5 mM BME), and then with 50 mM K-MES pH
403 6.6, 500 mM KCl, 5mM $MgCl_2$, 10% glycerol, 25 mM imidazole, 0.25 μM GTP, 5 mM BME) and
404 eluted in 50 mM K-MES pH 6.6, 500 mM KCl, 5mM $MgCl_2$, 10% glycerol, 250 mM imidazole,
405 0.25 μM GTP, 5 mM BME. Peak fractions were further purified with gel filtration (Superdex 200
406 10/300 GL) in buffer 50 mM K-MES pH 6.6, 500 mM KCl, 5 mM $MgCl_2$, 1 mM K-EGTA, 1 μM
407 GTP, 1 mM DTT.

408 All proteins were flash-frozen and stored at -80°C, and their concentration was determined
409 by analyzing a Coomassie-stained SDS-PAGE against known concentration of BSA (A7906,
410 Sigma).

411

412 **Purification, biotinylated and fluorescent labeling of γ-TuRC**

413 Endogenous γ-TuRC was purified from *Xenopus* egg extracts and labeled with the following steps
414 at 4°C. 7-8 ml of meiotic extract from *Xenopus* laevis eggs, prepared as described previously[45,46],
415 was first diluted 5-fold with CSF-XBg buffer (10mM K-HEPES, 100mM KCl, 1mM $MgCl_2$, 5mM
416 K-EGTA, 10% w/v sucrose, 1mM DTT, 1mM GTP, 10 μg/ml LPC protease inhibitors, pH 7.7),
417 centrifuged to remove large aggregates at 3500 rpm (Thermo Sorvall Legend XTR) for 10 minutes,
418 and the supernatant filtered sequentially with 1.2 μm and 0.8 μm Cellulose Acetate filters

419 (Whatman) followed by 0.22 μm PES filter (ThermoFisher). γ-TuRC was precipitated by
420 incubating with 6.5% w/v PEG-8000k (Sigma) for 30 minutes and centrifuged at 17,000 rpm (SS-
421 34 rotor, ThermoScientific) for 20 minutes. γ-TuRC-rich pellet was resuspended in CSF-XB buffer
422 with 0.05% v/v NP-40 using a mortar & pestel homogenizer, PEG was removed via centrifugation
423 at 136,000 xg for 7 minutes in TLA100.3 (Beckman Ultracentrifuge), and supernatant was pre-
424 cleared by incubating with Protein A Sepharose beads (GE LifeSciences #17127901) for 20
425 minutes. Beads were removed, γ-TuRC was incubated with 4-5 mg of a polyclonal antibody
426 custom-made against C-terminal residues 413-451 of *X. laevis* γ-tubulin (Genscript) for 2 hours
427 on gentle rotisserie, and further incubated with 1ml washed Protein A Sepharose bead slurry for 2
428 hours. γ-TuRC-bound beads were washed sequentially with 30 ml of CSF-XBg buffer, 30 ml of
429 CSF-XBg buffer with 250 mM KCl (high salt wash), 10 ml CSF-XBg buffer with 5mM ATP
430 (removes heat-shock proteins), and finally 10 ml CSF-XBg buffer before labeling. For
431 biotinylation of γ-TuRC, beads were incubated with 25 μM NHS-PEG4-biotin (A39259,
432 ThermoFisher) in CSF-XBg buffer for 1 hour at 4°C, and unbound biotin was removed by washing
433 with 30 ml CSF-XBg buffer prior to elution step. For combined fluorescent and biotin labeling of
434 γ-TuRC, the wash step after ATP-wash consisted of 10 ml of labelling buffer (10mM K-HEPES,
435 100mM KCl, 1mM $MgCl_2$, 5mM K-EGTA, 10% w/v sucrose, 0.5mM TCEP, 1mM GTP, 10 μg/ml
436 LPC, pH 7.2) and fluorescent labelling was performed by incubating the beads with 1 μM Alexa-
437 568 C_5 Maleimide (A20341, ThermoFisher). Unreacted dye was removed with 10 ml CSF-XBg
438 buffer, beads were incubated with 25 μM NHS-PEG4-biotin (A39259, ThermoFisher) in CSF-
439 XBg buffer for 1 hour at 4°C, and unreacted biotin removed with 30 ml CSF-XBg buffer. Labeled
440 γ-TuRC was eluted by incubating 2-3ml of γ-tubulin peptide (residues 413-451) at 0.4mg/ml in
441 CSF-XBg buffer with beads overnight. After 10-12 hours, γ-TuRC was collected by adding 1-2ml

442 CSF-XBg buffer to the column, concentrated to 200 µl in 30k NMWL Amicon concentrator (EMD
443 Millipore) and layered onto a continuous 10-50 w/w % sucrose gradient prepared in a 2.2 ml ultra-
444 clear tube (11x34 mm, Beckman Coulter) using a two-step program in Gradient Master 108
445 machine. Sucrose gradient fractionation of γ-TuRC was performed by centrifugation at 200,000xg
446 in TLS55 rotor (Beckman Coulter) for 3 hours. The gradient was fractionated from the top in 11-
447 12 fractions using wide-bore pipette tips and peak 2-3 fractions were identified by immunoblotting
448 against γ–tubulin with GTU-88 antibody (Sigma). γ-TuRC was concentrated to 80 µl in 30k
449 NMWL Amicon concentrator (EMD Millipore) and fresh purification was used immediately for
450 single molecule assays. Cryo-preservation of γ-TuRC molecules resulted in loss of ring assembly
451 and activity.
452
453 **Assessment of γ-TuRC with protein gel, immunoblot and negative stain electron microscopy**
454 To assess the purity of γ-TuRC, 3-5 µl of purified γ-TuRC was visualized on an SDS-PAGE with
455 SYPRO Ruby stain (ThermoFisher) following the manufacturer's protocol. Biotinylated subunits
456 of γ-TuRC were assessed by immunoblotting with Streptavidin-conjugated alkaline phosphatase
457 (S921, ThermoFisher). γ-TuRC purification was also assessed by visualizing using electron
458 microscopy. 4 µl of peak sucrose gradient fraction of γ-TuRC was pipetted onto CF400-Cu grids
459 (Electron Microscopy Sciences), incubated at room temperature for 60 seconds and then wicked
460 away. 2% uranyl acetate was applied to the grids for 30 seconds, wicked away, and the grids were
461 air-dried for 10 minutes. The grids were imaged using Phillips CM100 TEM microscope at 64000x
462 magnification.
463
464 **Preparation of functionalized coverslips**

465 22x22 mm, high precision coverslips (170±5 μm, Carl Zeiss, catalog # 474030-9020-000) were
466 functionalized for single molecule assays based on a recent protocol[23,47] with specific
467 modifications. Briefly, coverslips were labelled on the surface to be functionalized by scratching
468 "C" on right, bottom corner, placed in Teflon racks, sonicated with 3N NaOH for 30 minutes,
469 rinsed with water and sonicated in piranha solution (2 parts of 30 w/w % hydrogen peroxide and
470 3 parts sulfuric acid) for 45 minutes. Coverslips were rinsed thrice in water, and all water was
471 removed by spin drying completely in a custom-made spin coater. Pairs of coverslips were made
472 to sandwich 3-glycidyloxypropyl trimethoxysilane (440167, Sigma) on the marked sides, placed
473 in glass petri dishes, and covalent reaction was performed in a lab oven at 75°C for 30 minutes.
474 Coverslips were incubated for 15 minutes at room temperature, the sandwiches were separated,
475 incubated in acetone for 15 minutes, then transferred to fresh acetone and quickly dried under
476 nitrogen stream. Coverslip sandwiches were prepared with a small pile of well mixed HO-PEG-
477 NH_2 and 10% biotin-CONH-PEG-NH_2 (Rapp Polymere) in glass petri dishes, warmed to 75°C in
478 the lab oven until PEG melts, air bubbles were pressed out and PEG coupling was performed at
479 75°C overnight. The following day, individual coverslips were separated from sandwiches,
480 sonicated in MilliQ water for 30 minutes, washed further with water until no foaming is visible,
481 dried with a spin dryer, and stored at 4°C. Functionalized coverslips were used within 1 month of
482 preparation.

483 Imaging chambers were prepared by first assembling a channel on glass slide with double
484 sided tape strips (Tesa) 5 mm apart, coating the channel with 2mg/ml PLL(20)-g[3.5]- PEG(2)
485 (SuSOS) in dH_2O, incubating for 20 minutes, rinsing out the unbound PEG molecules with dH_2O
486 and drying the glass slide under the nitrogen stream. A piece of functionalized coverslip was cut

487 with the diamond pen and assembled functionalized face down on imaging chamber. The prepared
488 chambers were stored at 4°C and used within a day of assembly.
489
490 **Microtubule nucleation assay with purified γ-TuRC, microscopy and data analysis**
491 The imaging channel was prepared as follows. First, 5% w/v Pluronic F-127 in dH_2O was
492 introduced in the chamber (1 vol = 50 µl) and incubated for 10 minutes at room temperature. The
493 chamber was washed with 2 vols of assay buffer (80mM K-PIPES, 1mM $MgCl_2$, 1mM EGTA,
494 30mM KCl, 0.075% w/v methylcellulose 4000 cp, 1% w/v D-(+)-glucose, 0.02% w/v Brij-35,
495 5mM BME, 1mM GTP) with 0.05 mg/ml κ-casien (casein buffer), followed by 1 vol of 0.5 mg/ml
496 NeutrAvidin (A2666, ThermoFisher) in casein buffer, incubated on a cold block for 3 minutes,
497 and washed with 2 vols of BRB80 (80mM K-PIPES, 1mM $MgCl_2$, 1mM EGTA pH 6.8). 5-fold
498 dilution of γ-TuRC in BRB80 was introduced in the flow chamber and incubated for 10 minutes.
499 Unattached γ-TuRC molecules were washed with 1 vol of BRB80.
500 During the incubations, nucleation mix was prepared containing desired concentration of
501 αβ-tubulin (3.5-21 µM) purified from bovine brain with 5% Cy5-labeled tubulin along with
502 1mg/ml BSA (A7906, Sigma) in assay buffer, centrifuged for 12 minutes in TLA100 (Beckman
503 Coulter) to remove aggregates, a final 0.68 mg/ml glucose oxidase (SERVA, catalog # SE22778),
504 0.16 mg/ml catalase (Sigma, catalog # SRE0041) was added, and reaction mixture was introduced
505 into the flow chamber containing γ-TuRC.
506
507 **Total internal reflection fluorescence (TIRF) microscopy and analysis of microtubule**
508 **nucleation from γ-TuRC**

509 Nucleation of MTs was visualized with inverted Nikon TiE TIRF microscope using a 100X, 1.49
510 NA TIRF objective. An objective heater collar was attached (Bioptechs, model 150819-13) and
511 the temperature set-point of 33.5°C was used for experiments. Time-lapse videos were recorded
512 for 10 minutes at 0.5-1 frame per second using Andor iXon DU-897 camera with EM gain of 300
513 and exposure time of 50-200 ms each frame. Reference time-point zero (0 seconds) refers to when
514 the reaction was incubated at 33.5°C on the microscope, and for most reactions, imaging was
515 started within 30 seconds.

516 Growth speed of the plus-ends of MTs nucleated by γ-TuRC was measured by generating
517 kymographs in ImageJ. Region of interest (ROI) for individual MTs were selected and resliced to
518 generate length-time plot, a line was fit to the growing MT, the slope of line represents growth
519 speed. The kinetics of MT nucleation from γ-TuRC was measured as follows. A kymograph was
520 generated for every MT nucleated in the field of view. For most nucleation events, the time of
521 nucleation of the MT was obtained from observing the kymograph and manually recording the
522 initiation time point (see Fig. 1C for examples). For MTs where nucleation occurred before the
523 timelapse movie began or where the initiation was not clearly observed in the kymograph, the
524 shortest length of the MT that was clearly visible in the timelapse was measured and measured
525 average growth speed of MTs was used to estimate the time of nucleation. We verified that this
526 procedure accurately estimates the nucleation time for test case MTs where the nucleation event
527 was visible. The measurement of number of MTs ($N(t)$) nucleated versus time was generated from
528 a manual log containing the nucleation time for all MTs observed in the field of view, and a
529 representative set of curves is displayed in Fig. 1F. A straight line was fit to the initial (linear)
530 region of each $N(t)$ versus t curve, rate of nucleation was obtained slope of each linear fit, and its
531 power-law relation with tubulin concentration was obtained and reported (Fig. 1G).

532

533 **Spontaneous microtubule nucleation and data analysis**

534 Spontaneous MT assembly was visualized similar to γ-TuRC-mediated nucleation with the
535 following changes. The pluronic, casein and NeutrAvidin incubations were performed identical to
536 γ-TuRC nucleation assay but instead of attaching γ-TuRCs, sucrose-based buffer (of the same
537 composition as used for γ-TuRC elution) was diluted 5-fold with BRB80, introduced in the flow
538 chamber and incubated for 10 minutes. Washes were performed with 1 vol of BRB80, nucleation
539 mix was added, and imaging was performed as described above. MTs nucleate spontaneously in
540 solution fall down on the coverslip due to depletion forces during the 10 minutes of visualizing the
541 reaction. The number of MTs nucleated in the field of view were counted manually and plotted in
542 Fig. 1I.

543

544 **Preparation and microtubule assembly from blunt microtubule seeds**

545 Blunt MTs were prepared with GMPCPP nucleotide in two polymerization cycles as described
546 recently[22]. Briefly, a 50 μl reaction mixture was prepared with 20 μM bovine brain tubulin with
547 5% Alexa-568 labeled tubulin and 5% biotin-labeled tubulin, 1mM GMPCPP (Jena Bioscience)
548 in BRB80 buffer, incubated on ice for 5 minutes, then incubated on 37°C for 30 minutes to
549 polymerize MTs, and MTs were pelleted by centrifugation at 126,000 xg for 8 minutes at 30°C in
550 TLA100 (Beckman Coulter). Supernatant was discarded, MTs were resuspended in 80% original
551 volume of BRB80, incubated on ice for 20 minutes to depolymerize MTs, fresh GMPCPP was
552 added to final 1mM, incubated on ice for 5 minutes, a second cycle of polymerization was
553 performed by incubating the mixture at 37°C for 30 minutes, and MTs were pelleted again by
554 centrifugation. Supernatant was discarded and MTs were resuspended in 200 μl warm BRB80,

555 flash frozen in liquid nitrogen in 5μl aliquots, stored at -80°C and found to be stable for months.
556 To verify that these MT seeds have blunt ends, frozen aliquots were quickly thawed at 37°C,
557 diluted 20-fold with warm BRB80, and incubated at room temperature for 30 minutes to ensure
558 blunt ends as described previously[22]. MTs were pipetted onto CF400-Cu grids (Electron
559 Microscopy Sciences), incubated at room temperature for 60 seconds and then wicked away. 2%
560 uranyl acetate was applied to the grids for 30 seconds, wicked away, and the grids were air-dried
561 for 10 minutes. The grids were imaged using Phillips CM100 TEM microscope at 130000 x
562 magnification and most MT ends were found to be blunt.

563 To assay MT assembly from blunt MT seeds, MT assembly experiments similar to γ-TuRC
564 nucleation assays were performed with the following variation. A lower concentration 0.05 mg/ml
565 NeutrAvidin (A2666, ThermoFisher) was attached, and washes were performed with warm
566 BRB80 prior to attaching MTs. One aliquot of MT seeds was thawed quickly, diluted to 100-fold
567 with warm BRB80, incubated in the chamber for 5 minutes, unattached seeds were washed with 1
568 vol of warm BRB80, and the slide was incubated at room temperature for 30 minutes to ensure
569 blunt MT ends. Wide bore pipette tips were used for handling MT seeds to minimize the shear
570 forces that may result in breakage of MTs. Nucleation mix was prepared as described above and a
571 low αβ-tubulin concentration (1.4-8.7 μM) was used. MT assembly from blunt seeds was observed
572 immediately after incubating the slide on the objective heater. Imaging and analysis were
573 performed as described above for to γ-TuRC nucleation assays. However, the probability curves
574 for MT assembly were obtained (Fig. 2B) by normalizing for the total number of seeds observed
575 in the field of view. Rate of assembly was plotted against [tubulin concentration – C^*], where C^*
576 represents the critical tubulin concentration below which MT ends do not polymerize obtained
577 directly from experimental measurements (Fig. S2A-B).

578

579 **Electron microscopy of γ-tubulin filaments *in vitro***

580 Purified γ-tubulin was observed to form higher order oligomers previously using analytical gel
581 filtration[24]. γ-tubulin filaments were prepared by diluting pure γ-tubulin to 1-5 μM to the buffer
582 50mM K-MES pH 6.6, 5mM $MgCl_2$, 1mM EGTA, 100mM KCl. γ-tubulin mixture were pipetted
583 onto CF400-Cu grids (Electron Microscopy Sciences), incubated at room temperature for 60
584 seconds and then wicked away. 2% uranyl acetate was applied to the grids for 30 seconds, wicked
585 away, and the grids were air-dried for 10 minutes. The grids were imaged using Phillips CM100
586 TEM microscope at 130000 x magnification and γ-tubulin filaments were seen to form. At 500
587 mM KCl, γ-tubulin filaments were not seen.

588

589 **Nucleation of microtubules from purified γ-tubulin**

590 MT assembly experiments from purified γ-tubulin was performed similar to γ-TuRC nucleation
591 assays described above with following variation. No avidin was attached to the coverslips, and
592 varying concentration of γ-tubulin was prepared by diluting purified γ-tubulin in a high salt buffer
593 (50mM K-MES pH 6.6, 500mM KCl, 5mM $MgCl_2$, 1mM EGTA), centrifuging to remove
594 aggregates separately for 12 minutes in TLA100 before adding to the nucleation mix containing
595 15 μM αβ-tubulin (5% Cy5-labeled) with BSA, glucose oxidase and catalase as described above.
596 The reaction mixture was introduced into the flow chamber and imaged via TIRF microscopy. A
597 large number of MTs get nucleated immediately in the presence of 250 nM-1000 nM γ-tubulin.

598

599 **Measurement of affinity between purified γ-tubulin and αβ-tubulin**

600 Interaction assays between αβ-tubulin and γ-tubulin were performed with biolayer interferometry
601 using Octet RED96e (ForteBio) instrument in an 8-channel plate format. The plate temperature
602 was held at 33°C and the protein samples were shaken at 400 rpm during the experiment. First,
603 Streptavidin or anti-His antibody coated biosensors (ForteBio) were rinsed in interaction buffer
604 (50mM K-MES pH 6.6, 100mM KCl, 5mM $MgCl_2$, 1mM EGTA, 0.05% Tween20, 1mM GTP).
605 100 nM biotin-labeled αβ-tubulin, or blank buffer, was bound to Streptavidin sensor, or 200 nM
606 His-tagged γ-tubulin to anti-His sensor until loaded protein results in a wavelength shift (Δλ) of 3
607 nm. Unbound protein was removed by rinsing the sensor in interaction buffer, and interaction with
608 αβ-tubulin was measured by incubating the sensor containing αβ-tubulin, γ-tubulin or buffer with
609 0-35 μM unlabeled αβ-tubulin in interaction buffer for 5 minutes. Δλ (nm) was recorded as a
610 measure of the amount of unlabeled αβ-tubulin that binds to the sensor. Longitudinal interaction
611 occurs between αβ-tubulin dimers and the resulting protofilaments were verified by visualizing
612 the αβ-tubulin sample stained with 2% uranyl acetate using electron microscopy as described
613 above (Fig. S2D).
614
615 **Simulation of site occupation on γ-TuRC by αβ-tubulin dimers**
616 A simulation was performed in MATLAB for occupation of sites on γ-TuRC by αβ-tubulin dimers.
617 A circular grid was simulated with 13 empty positions that were occupied one per unit time
618 stochastically such that a new position was selected by uniform random number generator and
619 filled. If a previously filled position was selected, a different position was selected by the random
620 number generator. The sequence in which the sites were occupied was followed. For each
621 simulation, the total number of sites that were occupied when the first two neighboring sites are

622 filled was recorded. The simulation was repeated 10,000 times and the probability of occurrence
623 of first neighbor contact versus number of sites occupied is displayed in Fig. 2H.
624
625 **Measuring the effect of microtubule associated proteins on γ-TuRC's activity**
626 Effect of microtubule associated proteins (MAPs) was measured on γ-TuRC's nucleation activity.
627 γ-TuRC was attached on the coverslips using the setup described above and a control experiment
628 was performed with identical reaction conditions for each protein tested. Nucleation mix was
629 prepared containing 10.5 μM αβ-tubulin concentration (5% Cy5-labeled tubulin) as specified along
630 with 1mg/ml BSA and oxygen scavengers, and either buffer (control), 10nM GFP-TPX2, 100nM
631 EB1-mCherry, 5 μM Stathmin or 10nM MCAK was added. To test MCAK's effect, the assay
632 buffer additionally contained 1mM ATP. The reaction mixture containing tubulin and MAP at
633 specified concentration was introduced into the flow chamber containing γ-TuRC, and MT
634 nucleation was visualized by imaging the Cy5-fluorescent channel at 0.5-1 frames per second. For
635 TPX2 and EB1, fluorescence intensity of the protein was simultaneously acquired. The number of
636 MTs nucleated over time was measured as described above and the effect of protein on γ-TuRC's
637 nucleation activity was assessed by comparing nucleation curves with and without the MAP.
638 A similar set of experiments were performed to study the effect of XMAP215 on γ-TuRC-
639 mediated nucleation with the single molecule assays with the following differences. 20 nM of
640 XMAP215-GFP was added to nucleation mix prepared with 3.5-7 μM αβ-tubulin concentration
641 (5% Cy5-label) in XMAP assay buffer (80mM K-PIPES, 1mM $MgCl_2$, 1mM EGTA, 30mM KCl,
642 0.075% w/v methylcellulose 4000 cp, 1% w/v D-(+)-glucose, 0.007% w/v Brij-35, 5mM BME,
643 1mM GTP). MTs nucleated from attached γ-TuRC with and without XMAP215 were measured to
644 assess the efficiency of nucleation induced by XMAP215 (Fig. 3C). To assess if C-terminal of

645 XMAP215 increases nucleation efficiency, wild-type XMAP215 was replaced with a C-terminal
646 construct of XMAP215: TOG5-Cterminus-GFP in the described experiment.
647 To measure the kinetics of cooperative nucleation XMAP215 and γ-TuRC, a constant
648 density of γ-TuRC was attached as described above and nucleation mix nucleation mix was
649 prepared with a range of αβ-tubulin concentration between 1.6-7 μM (5% Cy5-label) with 20 nM
650 of XMAP215-GFP in XMAP assay buffer, introduced into reaction chamber and MT nucleation
651 was imaged immediately by capturing dual color images of XMAP215 and tubulin intensity at 0.5
652 frames per second.
653
654 **Triple-color imaging of XMAP215, γ-TuRC and microtubules**
655 For triple-color fluorescence assays (Fig. 3D), Alexa-568 and biotin-conjugated γ-TuRC was first
656 attached to coverslips as described above with the following variation: 0.05 mg/ml of NeutrAvidin
657 was used for attaching γ-TuRC. Nucleation mix was prepared with 7 μM αβ-tubulin (5% Cy5-
658 label), 10 nM Alexa-488 SNAP-tagged XMAP215 with BSA and oxygen scavengers in XMAP
659 assay buffer (80mM K-PIPES, 1mM $MgCl_2$, 1mM EGTA, 30mM KCl, 0.075% w/v
660 methylcellulose 4000 cp, 1% w/v D-(+)-glucose, 0.007% w/v Brij-35, 5mM BME, 1mM GTP)
661 and introduced into the reaction chamber containing attached γ-TuRC. Three-color imaging per
662 frame was performed with sequential 488, 568 and 647 nm excitation and images were acquired
663 with EMCCD camera at 0.3 frames per second.

664 **Figure legends**

665

666 **Figure 1. Microtubule nucleation by γ-TuRC.**

667 (A) Schematic of γ-TuRC mediated nucleation based on template model. (B) Purified, biotinylated
668 γ-TuRC molecules were attached and time-lapse of MT nucleation is shown. Arrows point to
669 nucleation sites. Representative kymographs of MTs nucleated from γ-TuRC are displayed in (C).
670 The experiment and analyses in (B-G) were repeated at least thrice with independent γ-TuRC
671 preparations. (D) Titrating tubulin concentration with constant the density of γ-TuRC. MT
672 nucleation from γ-TuRC begins at 7 μM tubulin. (E) MT plus-end growth speed increases linearly
673 with tubulin concentration. Linear fit (red line) with shaded 95% confidence intervals is displayed,
674 with critical concentration for polymerization as C^* = 1.4 μM. Inset: Number of MTs nucleated
675 by γ-TuRCs within 120 seconds varies non-linearly with tubulin concentration. (F) Number of
676 MTs nucleated ($N(t)$) over time (t) is plotted for varying tubulin concentration to obtain rate of
677 nucleation as the slope of the initial part of the curves. (G) Number of tubulin dimers (n) in the
678 critical nucleus on γ-TuRC was obtained as 3.7 ± 0.5 from the equation $\left.\frac{dN}{dt}\right|_{t\to 0} = kC_{tub}{}^{n}$
679 displayed on a log-log plot. Data from two independent experiments was pooled and reported. (H)
680 Spontaneous MT nucleation (schematized) was measured with increasing tubulin concentration
681 and high concentrations. 14 μM tubulin is required. (I) Number of MTs ($N(t=\tau)$) nucleated
682 spontaneously were plotted against tubulin concentration (C_{tub}). Power-law curve was fit as $N(t=\tau)$
683 $= k\ C_{tub}{}^{n}$ and tubulin cooperativity (exponent) of n = 8 ± 1 was obtained. Experiments were
684 repeated twice independently with many supporting results and all data were pooled. Scale bars,
685 10 μm. See Figure S1 and Movies S1-S4.

686

687 **Figure 2. Molecular mechanism for γ-TuRC-mediated microtubule nucleation.**

688 (A) Schematic and a micrograph of pre-formed, blunt MT seeds is shown and MT assembly from
689 them was observed (right) with varying tubulin concentration. (B) Cumulative probability of MT
690 assembly from seeds ($p(t)$) over time (t) is plotted and rate of nucleation was obtained as the slope
691 from initial part of the curves. (C) Tubulin dimers (n) needed for MT assembly from seeds was
692 from the relation $\left.\frac{dp}{dt}\right|_{t\to 0} = k(C_{tub} - C^*)^n$ displayed on a log-log plot. $n = 1.2 \pm 0.4$ showing non-
693 cooperative assembly of tubulin. (D) MTs nucleate from purified γ-tubulin oligomers efficiently
694 and (E) minus-ends of γ-tubulin-nucleated MTs remain capped while the plus-ends polymerize.
695 (F) Molecular interaction between γ/αβ-tubulin was probed with bio-layer interferometry. Buffer
696 (left), biotin-tagged αβ-tubulin (middle), or His-tagged γ-tubulin (right) were loaded on the probe
697 as bait and untagged αβ-tubulin at 0-35 μM as prey. Wavelength shift, $\Delta\lambda$ (nm) indicated no
698 binding between empty probe and αβ-tubulin or γ/αβ-tubulin, while that between αβ-/αβ-tubulin
699 was observed and confirmed to be longitudinal (protofilament-wise, Fig. S2D). (G) Interface
700 interaction model determines MT nucleation by γ-TuRC where lateral γ/γ-tubulin promote
701 nucleation while low γ/αβ-tubulin affinity tunes nucleation. (H) Simulations were conducted where
702 13 sites on γ-TuRC were stochastically occupied by αβ-tubulins. For two αβ-tubulin subunits to
703 form lateral bond by occupying neighboring sites, 3.7 ± 1 subunits bind on average on γ-TuRC,
704 predicting the size of critical nucleus. Experiments and analyses were repeated at least twice
705 independently with multiple supporting results. Scale bars, 10 μm. See Figure S2 and Movie S5-
706 6.

707

708 **Figure 3. Regulation of microtubule nucleation by TPX2 and XMAP215.**

709 (A) A constant density of γ-TuRC molecules were attached and 10.5μM tubulin ± 10nM GFP-
710 TPX2 were added. MTs were counted (right plot) and TPX2 was did not affect γ-TuRC-mediated
711 nucleation. Scale bar, 10μm. (B) γ-TuRCs were attached and low concentration 3.5-7μM ± 20nM
712 XMAP215 was added. XMAP215 induces MT nucleation from γ-TuRC efficiently. (C) MT
713 nucleation events were counted and plotted. Scale bar, 10μm. (D) Sequence of events during
714 cooperative MT nucleation by γ-TuRC and XMAP215 was visualized using labeled γ-TuRC
715 (blue), XMAP215 (red) and tubulin (green). Time-lapse: γ-TuRC and XMAP215 form a complex
716 prior to MT nucleation. XMAP215 variably resides on γ-TuRC for long (>100 seconds,
717 kymograph 1) or short times (~3-10 seconds, kymograph 2) before MT nucleation and remains at
718 the minus-end with 50% probability. Scale bar, 5μm. (E) Titrating tubulin with constant γ-TuRC
719 and XMAP215 concentration. XMAP215/γ-TuRC nucleate MTs from 1.6 μM tubulin. Number of
720 MTs nucleated ($N(t)$) over time (t) is plotted (inset) and rate of nucleation was obtained. Tubulin
721 dimers (n) in critical nucleus was obtained as 3.2 ± 1.2 and displayed on a log-log plot. The
722 experiment was performed once for all concentrations denoted and supported by a number of
723 additional experiments. The remaining experiments were repeated more than twice with
724 independent γ-TuRC preparations with additional supporting results. See Figure S3-4 and Movies
725 S7-10.
726

727 **Supplementary Figure legends**

728

729 **Supplementary Figure 1. Controls for γ-TuRC-mediated and spontaneous microtubule**
730 **nucleation.**

731 (A-B) Protein gel (left) of purified γ-TuRC was stained with SYPRO Ruby stain and biotinylated
732 sites on γ-TuRC visualized with alkaline phosphatase conjugated to avidin (right). Major, known
733 γ-TuRC components were detected in the purified protein and GCP2/3 are heavily biotinylated
734 during purification. Purified and biotinylated γ-TuRC was stained with uranyl acetate and
735 visualized with transmission electron microscopy. Scale bar, 100nm. The experiments were
736 repeated at least thrice with independent γ-TuRC preparations.

737 (C) Covalent-reaction of biotin with γ-TuRC does not affect the nucleation activity, as measured
738 by attaching γ-TuRC with anti-Mozart1 antibody and comparing the number of MTs nucleated by
739 untagged and biotinylated γ-TuRC. Scale bar, 10μm.

740 (D) Control reactions for γ-TuRC-mediated nucleation. MTs were nucleated by attaching purified
741 γ-TuRC (left), adding control buffer (middle) or missing avidin in the reaction sequence (right).
742 Robust MT nucleation only occurs with γ-TuRC attached to coverslips and not in control reactions.
743 Scale bar, 10μm. See Movie S2.

744 (E) MTs were first nucleated from γ-TuRC with Alexa 568-labeled tubulin (cyan), followed by
745 introduction of Cy5-labeled tubulin (magenta). New tubulin only incorporates on the freely
746 growing, plus-end but not at the nucleated minus-end. Scale bar, 10μm. The experiment was
747 performed more than three times.

748 (F) Two representative kymographs of spontaneously nucleated MTs are displayed, demonstrating
749 that MTs grow from both the minus-end (dotted line) and the plus-end (solid line). Scale bar,
750 10μm. See Movie S4.
751 (G) MTs nucleation from γ-TuRCs or spontaneously were compared at two tubulin
752 concentrations: 10.5 μM and 14 μM. γ-TuRC nucleates 10-fold higher number of MTs than
753 spontaneous assembly. The experiment was performed twice with many supporting results.
754 See also Figure 1.
755
756 **Supplementary Figure 2. Microtubule assembly from blunt seeds and filament formation by**
757 **purified γ-tubulin.**
758 (A) MT assembly (magenta) from MT seeds with blunt ends (cyan) was assayed. Tubulin
759 concentration was titrated, and MT plus-end assembles starting from 2.45 μM tubulin, which is
760 only slightly above the critical concentration of polymerization. Scale bar, 10μm.
761 (B) Growth speed of MT plus-ends was measured from kymographs and critical concentration (C^*
762 = 1.4 μM) was determined from the linear fit (red line) with shaded 95% confidence intervals. The
763 experiment and analyses in were repeated twice on independent days along with other supporting
764 data. See also Figure 2 and Movie S5.
765 (C) γ-tubulin self-assembles into filaments at high concentration and low-salt (100mM KCl) as
766 imaged with negative-stain electron microscopy, whereas γ-tubulin filaments were not observed
767 at high-salt (500mM KCl). Scale bar, 100nm.
768 (D) Transmission electron microscopy of bio-layer interferometry assay of Fig. 2F show that
769 protofilaments of αβ-tubulin form. The experiment was repeated twice. Scale bar, 100nm.
770

771 **Supplementary Figure 3. Effect of microtubule associated proteins on γ-TuRC-mediated**
772 **nucleation.**
773 (A) γ-TuRC molecules were attached to coverslips and either tubulin alone (pseudo-colored as
774 magenta, left) or tubulin with 100nM EB1-mCherry (pseudo-colored as cyan, right) was added to
775 the reaction. Number of MTs nucleated were measured (right plot) and EB1 was observed to
776 neither increase nor decrease γ-TuRC-mediation nucleation despite functioning as a catastrophe
777 factor *in vitro*. The experiment was repeated at least twice with independent γ-TuRC preparation.
778 See also Movie S8. Scale bar, 10μm.
779 (B) γ-TuRC molecules were attached to coverslips and either tubulin alone (left images), tubulin
780 with 10nM MCAK (top right) or tubulin with 5μM Stathmin (bottom right) was added to the
781 reaction. Both MCAK and Stathmin were observed to decrease the number of MTs nucleated
782 because of their role in decreasing the net polymerization of a MT. The experiment was repeated
783 at least twice with independent γ-TuRC preparations. Scale bar, 10μm.
784
785 **Supplementary Figure 4. Cooperative microtubule nucleation XMAP215 and γ-TuRC.**
786 (A) γ-TuRC molecules were attached and increasing concentration of tubulin was added with
787 20nM XMAP215. XMAP215 was found to induce MT nucleation from γ-TuRC molecules at even
788 low tubulin concentration of 1.6-3.5 μM where γ-TuRCs alone do not nucleate MTs. See Figure
789 3E. Scale bar, 10μm.
790 (B) The role of C-terminal region of XMAP215 was tested in cooperative nucleation with γ-TuRC.
791 MTs nucleated by γ-TuRC alone (left), γ-TuRC with 20nM full-length XMAP215 (middle) or γ-
792 TuRC with 20nM C-terminal domain of XMAP215 were visualized. The C-terminal domains of

793 XMAP215 do not stimulate MT nucleation from γ-TuRC. The experiment was repeated twice with

794 independent γ-TuRC preparations. Scale bar, 10μm.

795

796 **Movie Legends**

797

798 **Movie 1. Microtubule nucleation from γ-TuRC complexes**

799 γ-TuRC was attached to functionalized coverslips and MT nucleation was observed upon
800 introducing fluorescent αβ-tubulin (gray). MTs nucleated from individual γ-TuRC molecules from
801 zero length at 15μM αβ-tubulin and the plus-end of nucleated MTs polymerized, but not its minus-
802 end. Elapsed time is shown in seconds, where time-point zero represents the start of reaction. Scale
803 bar, 10 μm.

804

805 **Movie 2. Microtubule nucleation from γ-TuRC is specific**

806 γ-TuRC was immobilized on coverslips (leftmost panel) and MT nucleation was observed upon
807 introducing fluorescent αβ-tubulin (gray). Control reactions where either no γ-TuRC was added
808 (middle panel) or γ-TuRC was not specifically attached (rightmost panel) did not result in MT
809 nucleation. Elapsed time is shown in seconds, where time-point zero represents the start of
810 reaction. Scale bar, 10 μm.

811

812 **Movie 3. γ-TuRC molecules nucleated microtubules efficiently**

813 Constant density of γ-TuRC was attached while concentration of fluorescent αβ-tubulin was
814 titrated (3.5-21μM) and MT nucleation was observed. γ-TuRC molecules nucleated MTs starting
815 from 7μM tubulin and MT nucleation increased non-linearly with increasing tubulin concentration.
816 Elapsed time is shown in seconds, where time-point zero represents the start of reaction. Scale bar,
817 10 μm.

818

819 **Movie 4. Spontaneous microtubule nucleation occurs at high tubulin concentration**

820 Concentration of fluorescent αβ-tubulin was titrated (7-21μM) and spontaneous MT nucleation
821 was assayed. MTs nucleated spontaneously starting from high concentration of 14μM tubulin and
822 MT nucleation increased non-linearly with tubulin concentration. Both plus- and minus-ends of
823 the assembled MTs polymerize. Elapsed time is shown in seconds, where time-point zero
824 represents the start of reaction. Scale bar, 10 μm.

825

826 **Movie 5. Microtubule assembly from blunt plus-ends resembles polymerization**

827 MTs with blunt ends (seeds, cyan) were generated and attached to functionalized coverslips.
828 Varying concentration of fluorescent αβ-tubulin was added (1.4-8.7μM, pseudo-colored as
829 magenta) and MT assembly from seeds was assayed. MTs assembled at concentration above
830 1.4μM tubulin, which is the minimum concentration needed for polymerization of MT plus-ends
831 (*C**). MT assembly from seeds increased linearly with the concentration of assembly-competent
832 tubulin (*C-C**). Elapsed time is shown in seconds, where time-point zero represents the start of
833 reaction. Scale bar, 10 μm.

834

835 **Movie 6. Arrays of purified γ-tubulin nucleate microtubules**

836 Purified γ-tubulin nucleated MTs. Fluorescent αβ-tubulin (10.5μM, colored as gray) was added to
837 purified γ-tubulin at increasing concentration, and MT nucleation was assessed. MTs assembled
838 from 250-1000 nM γ-tubulin, where γ-tubulin alone self-assembled into higher order oligomers
839 and filaments in lateral γ/γ-tubulin arrays. Minus-ends of γ-tubulin-nucleated MTs did not
840 polymerize, while the plus-ends did. Elapsed time is shown in seconds, where time-point zero
841 represents the start of reaction. Scale bar, 10 μm.

842

843 **Movie 7. TPX2 does not increase γ-TuRC's microtubule nucleation activity**

844 γ-TuRC was immobilized on coverslips and MT nucleation was observed upon introducing
845 fluorescent αβ-tubulin (10.5μM, pseudo-colored as magenta) without or with 10nM GFP-TPX2
846 (pseudo-colored as cyan) in the left and right panels respectively. TPX2 bound along the nucleated
847 MTs but did not increase the MT nucleation activity of γ-TuRC molecules. Elapsed time is shown
848 in seconds, where time-point zero represents the start of reaction. Scale bar, 10 μm.

849

850 **Movie 8. EB1 does not decrease the microtubule nucleation activity of γ-TuRC**

851 γ-TuRC was immobilized on coverslips and MT nucleation was observed upon introducing
852 fluorescent αβ-tubulin (10.5μM, pseudo-colored as magenta) without or with 100nM EB1-
853 mCherry (pseudo-colored as cyan) in the left and right panels respectively. EB1 binds the plus-
854 ends of nucleated MTs but did not decrease the MT nucleation activity of γ-TuRC molecules.
855 Elapsed time is shown in seconds, where time-point zero represents the start of reaction. Scale bar,
856 10 μm.

857

858 **Movie 9. XMAP215 increases microtubule nucleation activity of γ-TuRC**

859 γ-TuRC was immobilized on coverslips and MT nucleation was assayed with low concentration
860 of fluorescent αβ-tubulin (3.5μM and 7μM) without (top panels) or with 20nM XMAP215-GFP
861 (bottom panels). XMAP215 decreased the minimal concentration of tubulin necessary to induce
862 MT nucleation from γ-TuRC. Elapsed time is shown in seconds, where time-point zero represents
863 the start of reaction. Scale bar, 10 μm.

864

865 **Movie 10. Synergistic microtubule nucleation by γ-TuRC and XMAP215**

866 Triple-color fluorescence microscopy was performed to observe the molecular sequence of events
867 during MT nucleation from γ-TuRC and XMAP215. γ-TuRC (blue) and XMAP215 (red) formed
868 a complex before MT nucleation occurred (pseudo-colored as green). For 50% of these events,
869 XMAP215 remains on the nucleated minus-end. Elapsed time is shown in seconds, where time-
870 point zero represents the start of reaction. Scale bar, 10 μm.

871

Figure 1

A γ-TuRC-mediated microtubule nucleation

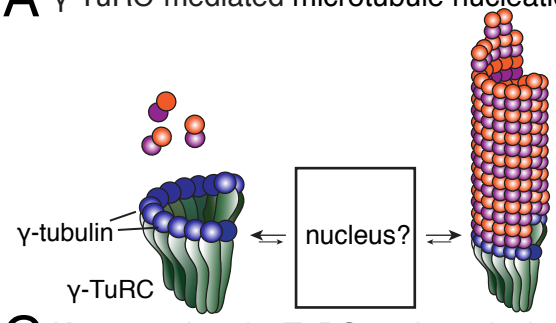

B Microtubule nucleation from γ-TuRC *in vitro*

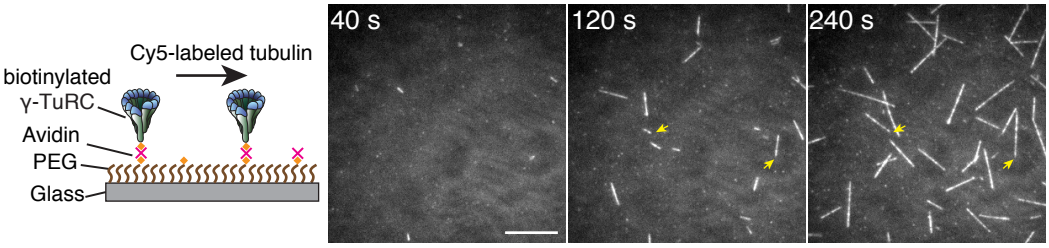

C Kymographs of γ-TuRC nucleated microtubules

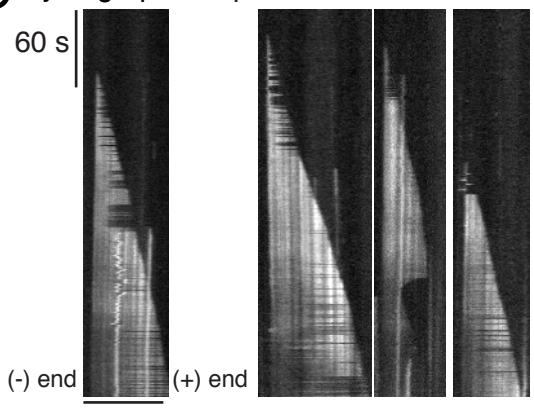

D Titrating tubulin concentration in γ-TuRC-mediated nucleation

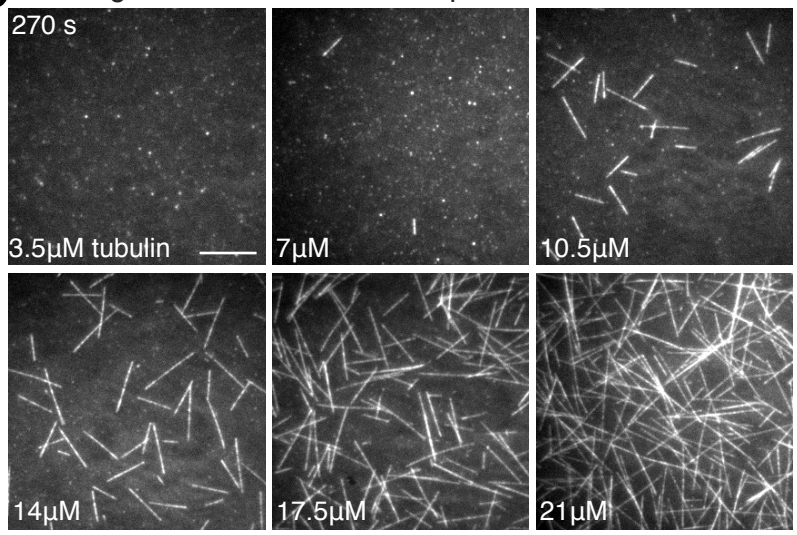

E Growth speed of plus-end and number of microtubules

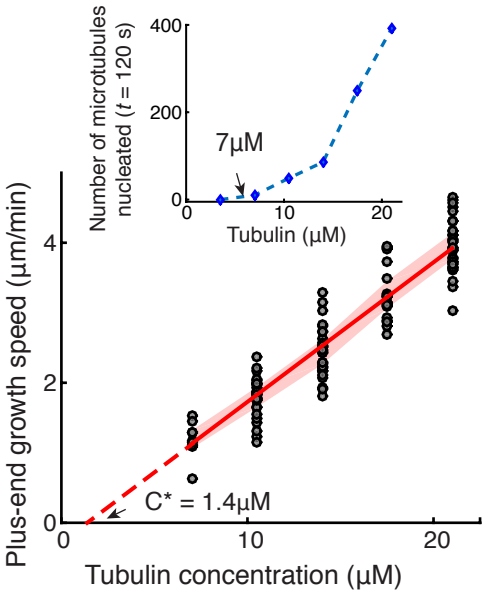

F Kinetics of microtubule nucleation from γ-TuRC

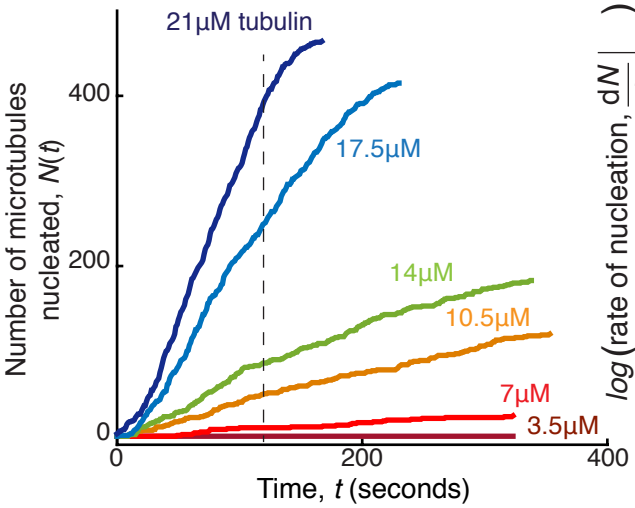

G Cooperativity of tubulin dimers for γ-TuRC mediated nucleation (*n*)

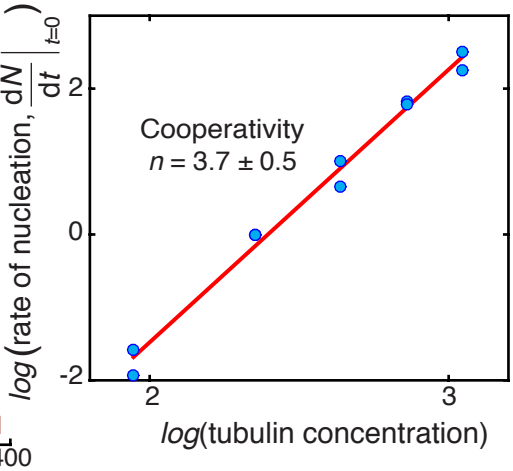

H Spontaneous microtubule nucleation

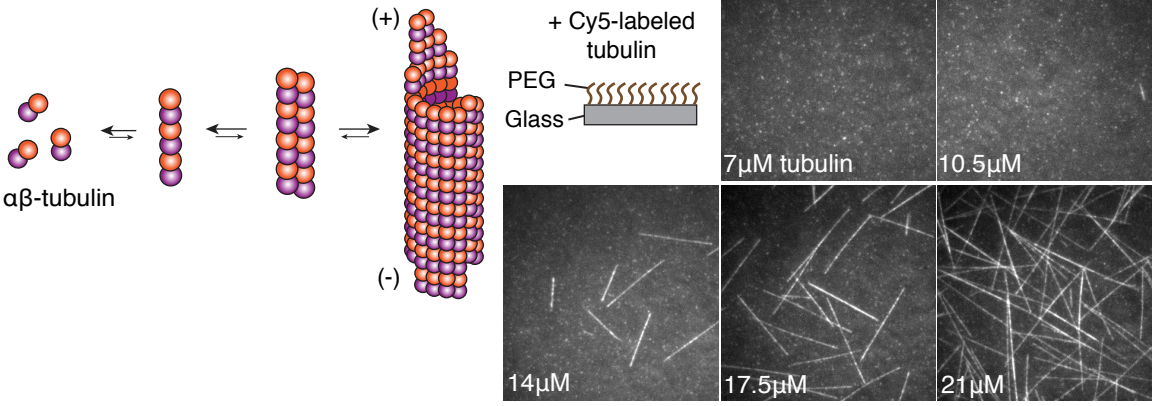

I Cooperativity of tubulin dimers for spontaneous nucleation (*n*)

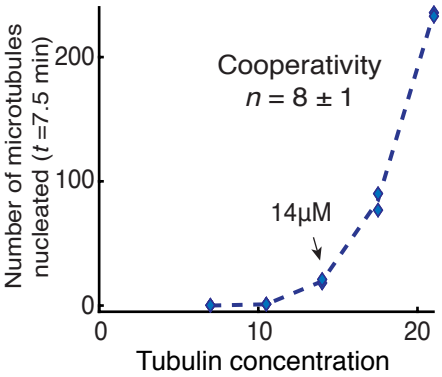

Figure 2

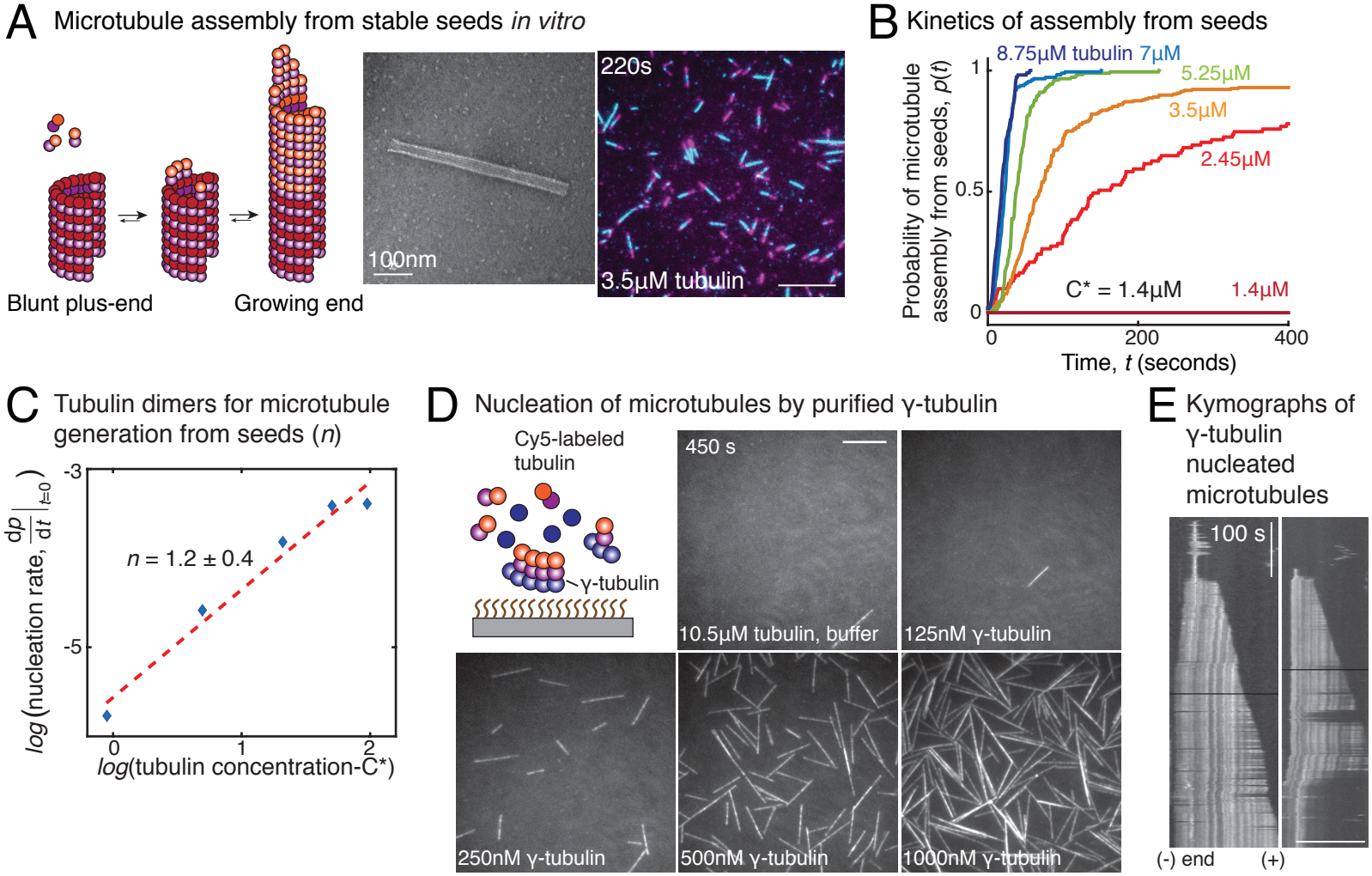
A Microtubule assembly from stable seeds in vitro
Blunt plus-end
Growing end
100nm
220s
3.5μM tubulin
B Kinetics of assembly from seeds
8.75μM tubulin 7μM
5.25μM
3.5μM
2.45μM
C* = 1.4μM
1.4μM
Probability of microtubule assembly from seeds, p(t)
Time, t (seconds)
C Tubulin dimers for microtubule generation from seeds (n)
n = 1.2 ± 0.4
log(nucleation rate, dp/dt |t=0)
log(tubulin concentration-C*)
D Nucleation of microtubules by purified γ-tubulin
Cy5-labeled tubulin
γ-tubulin
450 s
10.5μM tubulin, buffer
125nM γ-tubulin
250nM γ-tubulin
500nM γ-tubulin
1000nM γ-tubulin
E Kymographs of γ-tubulin nucleated microtubules
100 s
(-) end
(+)
F Probing interaction between γ-tubulin and αβ-tubulin
Blank
αβ-tubulin
γ-tubulin
0-35μM tubulin
Δλ (nm)
Time (s)
G Interface interaction model
αβ-tubulin
γ-tubulin
lower affinity
higher affinity
H Simulation of αβ-tubulin binding on γ-TuRC sites
Available sites on γ-TuRC
Occupying sites at random
Neighbours = lateral αβ-tubulin contacts
Probability of lateral αβ-tubulin contacts
<n> = 3.7 ± 1
Number of sites occupied (n)

Figure 3

A TPX2 does not influence γ-TuRC-mediated nucleation

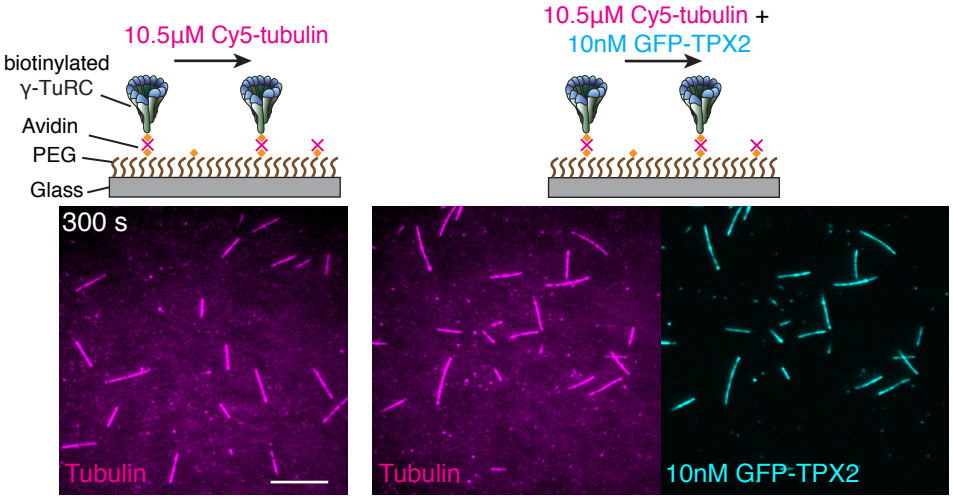

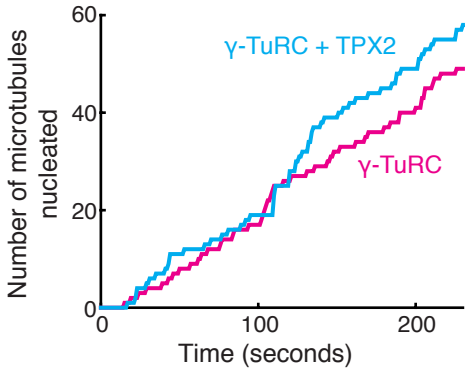

B XMAP215 decreases the nucleation barrier from γ-TuRCs

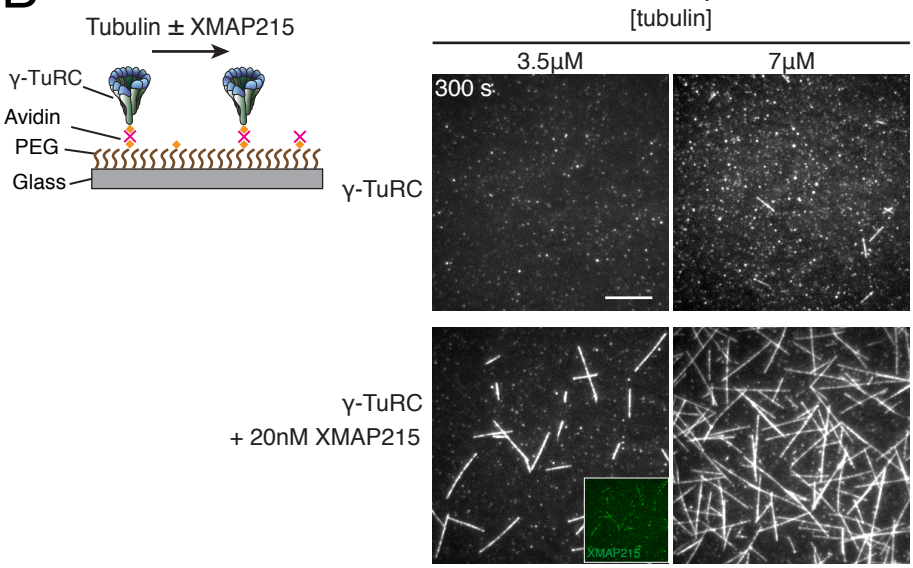

C Kinetics of microtubule nucleation from γ-TuRC with XMAP215

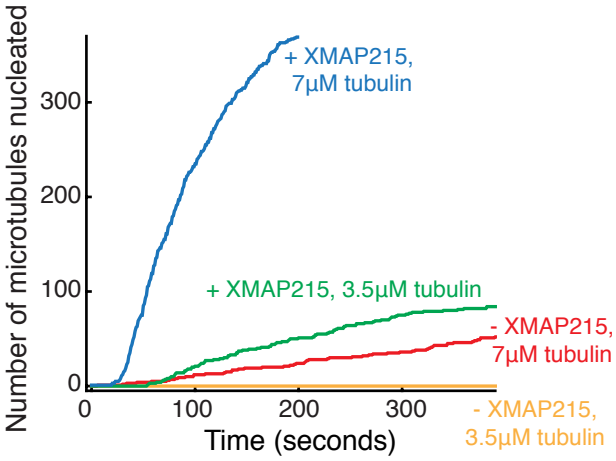

D XMAP215 binds γ-TuRC prior to microtubule nucleation

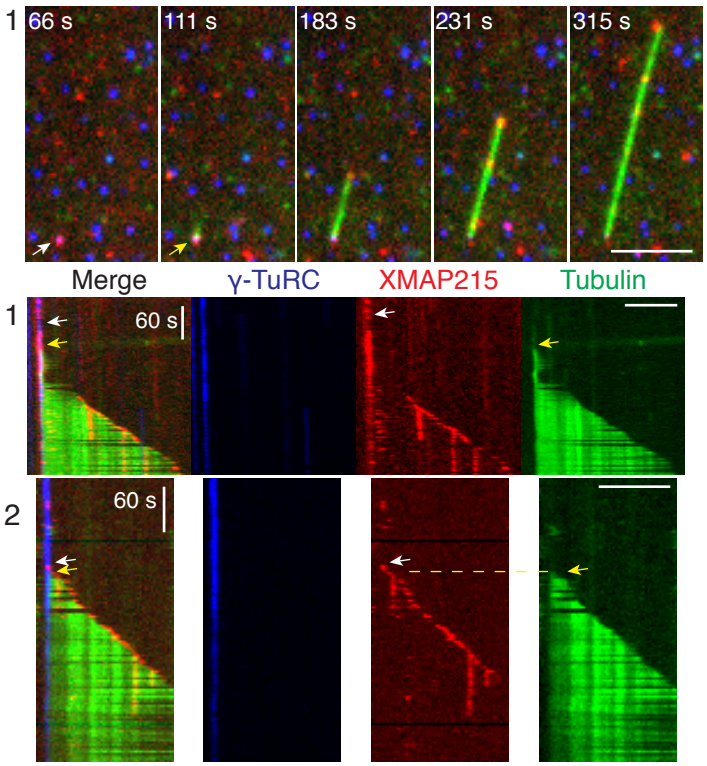

E Cooperativity of tubulin dimers for co-nucleation by γ-TuRC and XMAP215 (*n*)

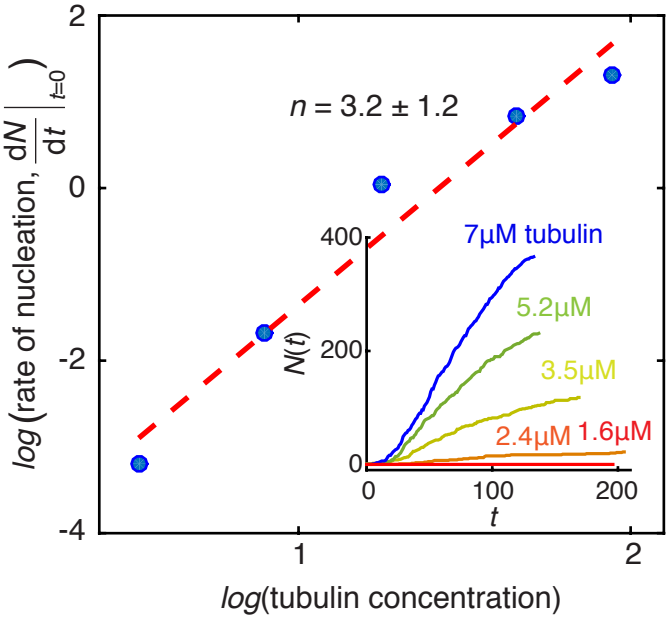

Figure S1 γ-TuRC purification and quality control reactions

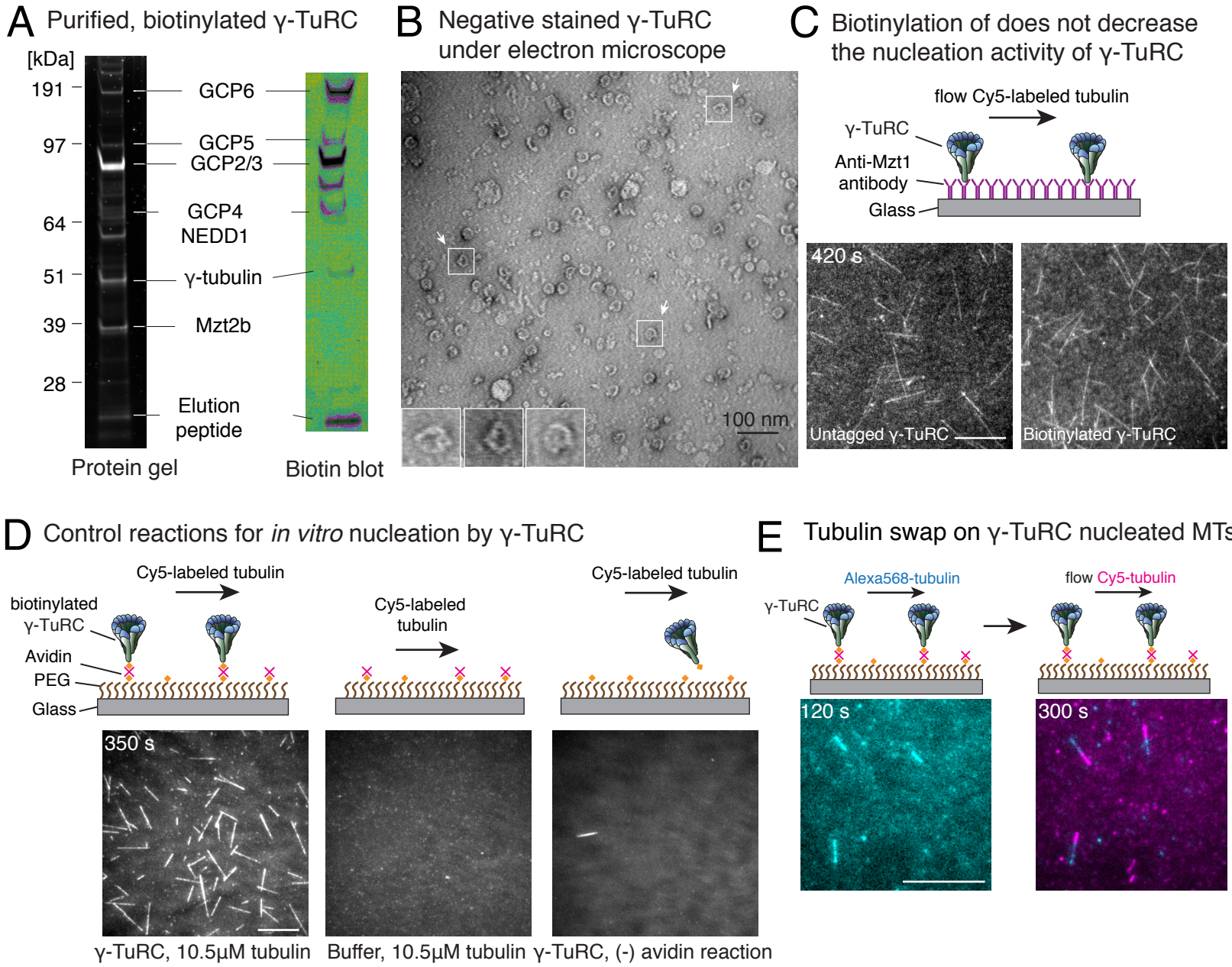

Figure S2

A Titrating tubulin on stable microtubule seeds

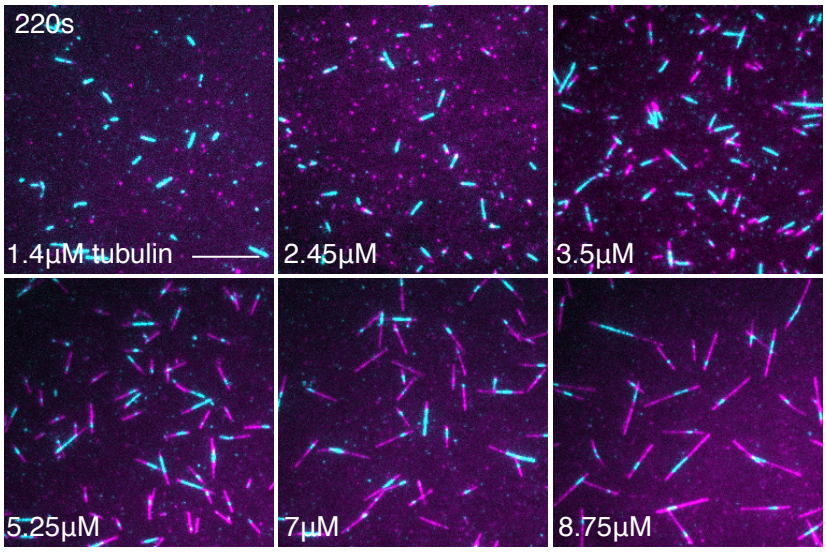

B Growth speed of microtubule plus-ends

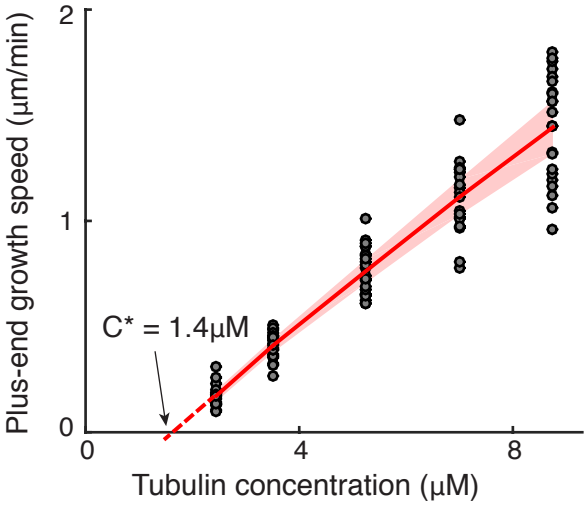

C γ-tubulin filaments form under physiological salt at high concentration *in vitro*

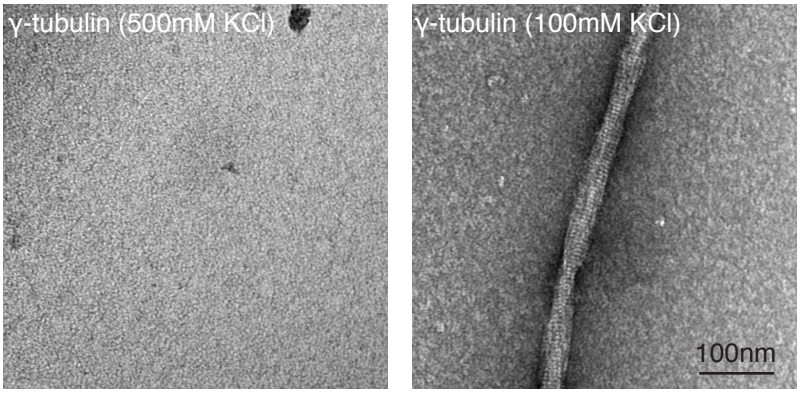

D αβ-tubulin protofilaments form under biolayer interferometry

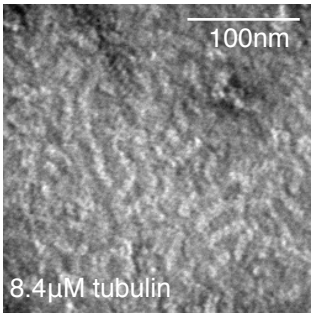

Figure S3

A Effect of EB1 on γ-TuRC-mediated nucleation

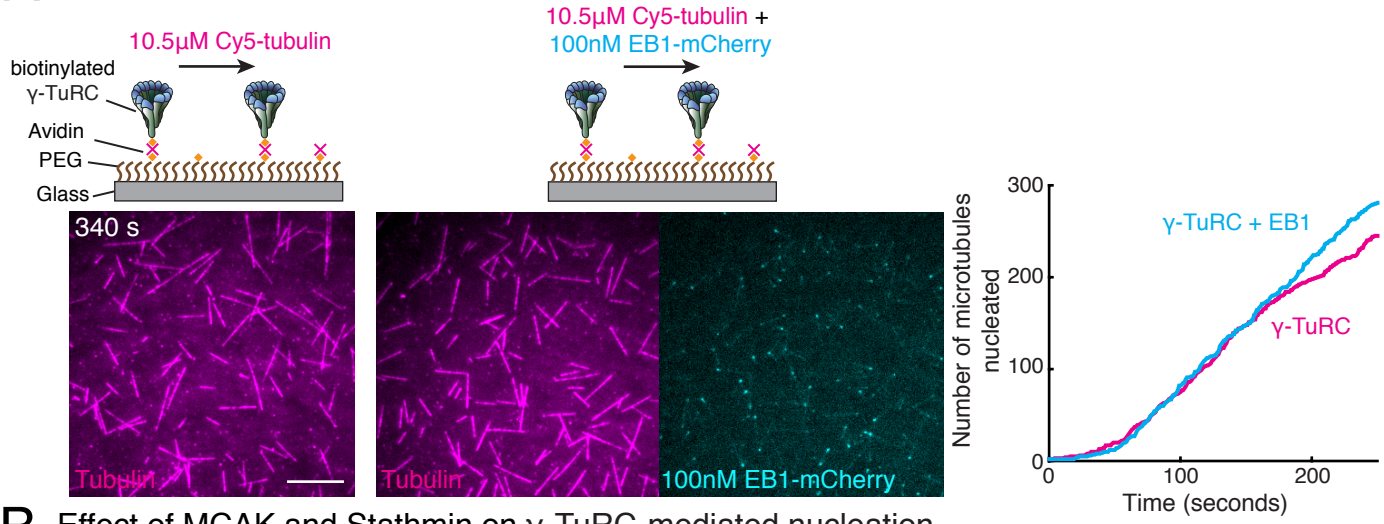

B Effect of MCAK and Stathmin on γ-TuRC-mediated nucleation

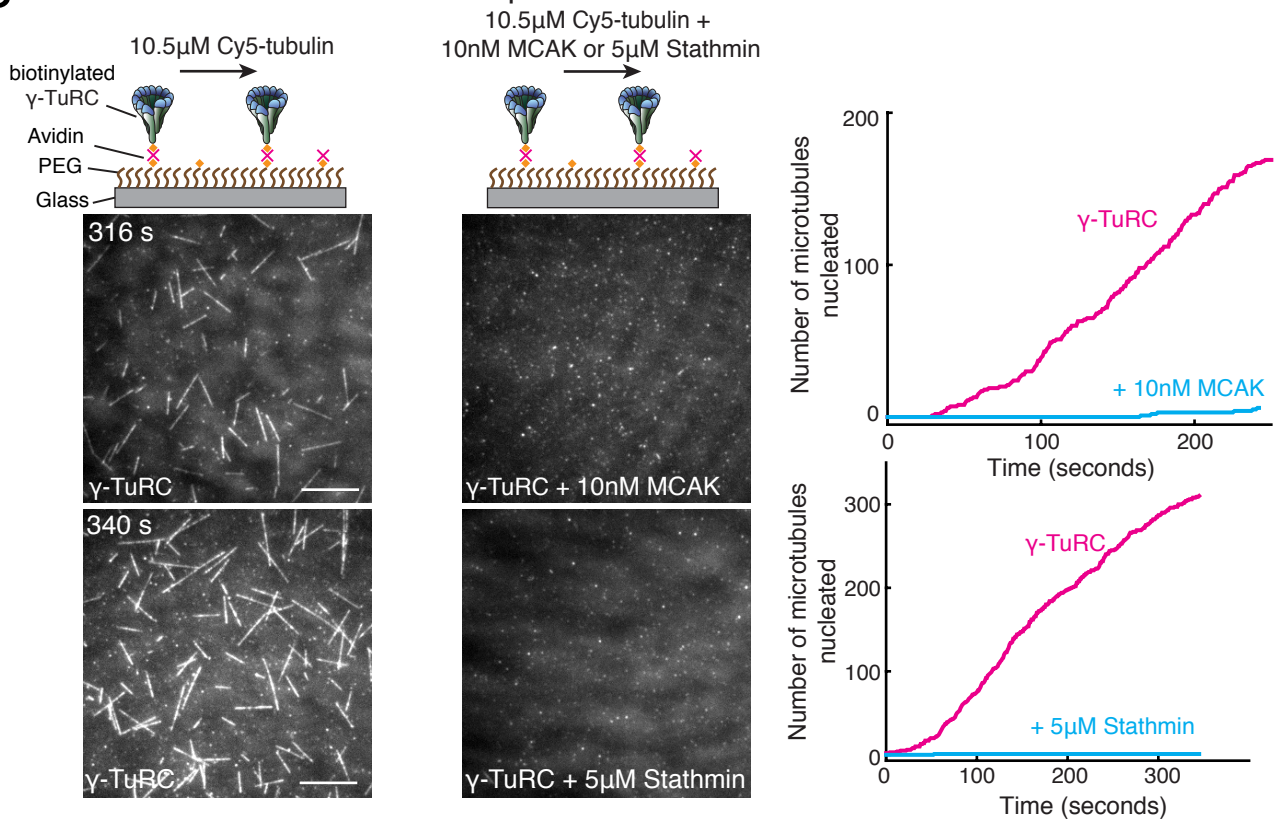

Figure S4

A Titrating tubulin concentration in γ-TuRC/XMAP215-mediated co-nucleation

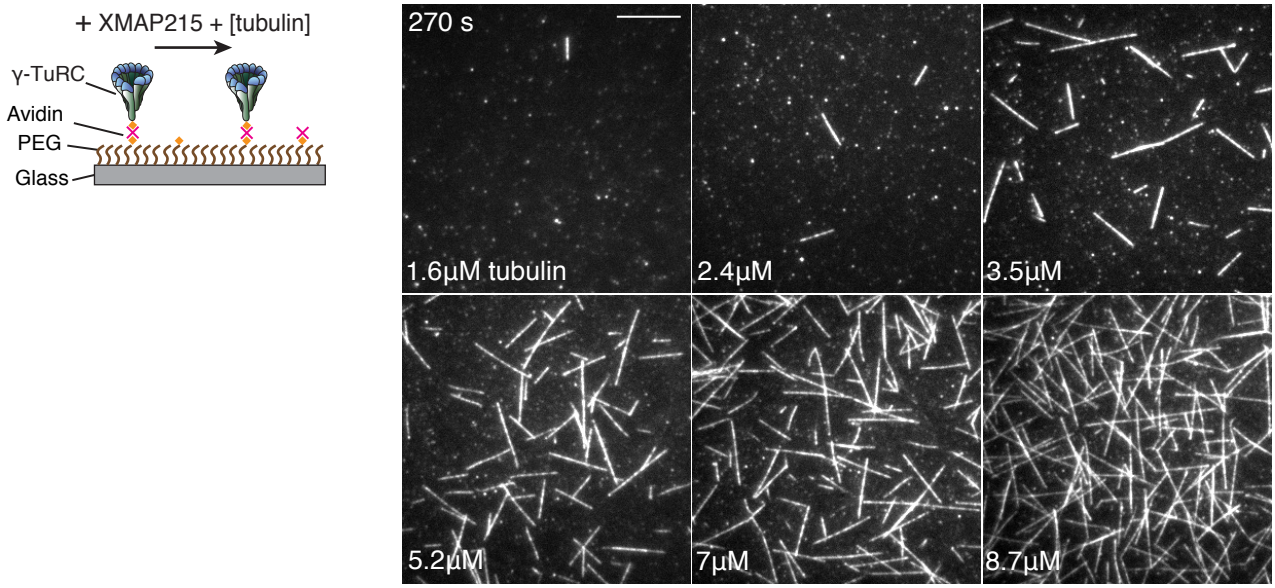
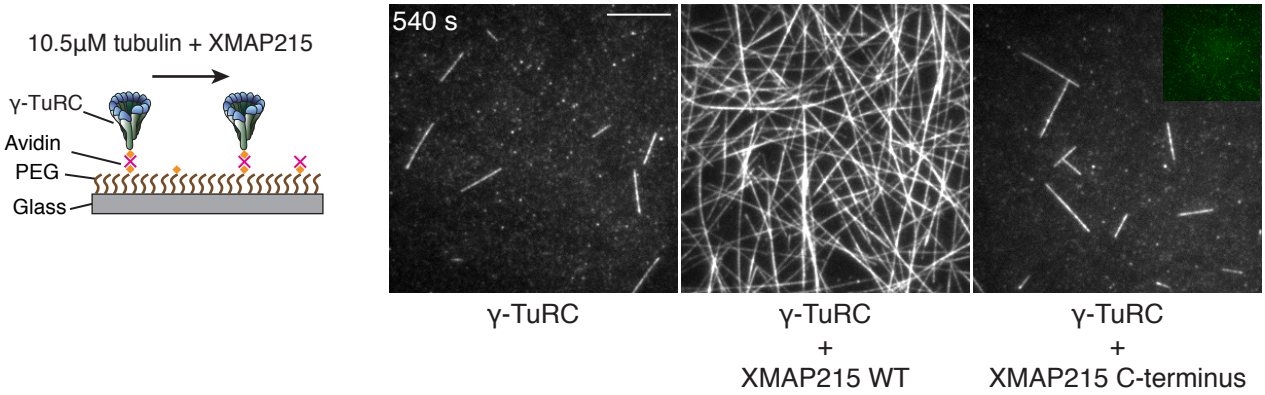
B C-terminal region of XMAP215 does not stimulate nucleation from γ-TuRC